LITHOS 434-435 (2022) 106944

Contents lists available at ScienceDirect

LITHOS

journal homepage: www.elsevier.com/locate/lithos

# Subducted oceanic plateau fed crustal growth: Insights from Amdo dacites in central Tibetan Plateau

Haiyan Fan [a], Man Zhang [a,1], Feng Huang [a,*], Jifeng Xu [a,b], Xijun Liu [b], Yunchuan Zeng [a], Song Zhang [a], Qian Liu [c], Mingda Lv [d], Hongxia Yu [b], Ye Tian [a], Liying Zhang [a], Ting Zhou [e], Zhenglin Li [b], Yinhui Zhang [b]

[a] State Key Laboratory of Geological Processes and Mineral Resources, and School of Earth Science and Resources, China University of Geosciences, Beijing 100083, China
[b] Guangxi Key Laboratory of Hidden Metallic Ore Deposits Exploration, Guilin University of Technology, Guilin 541004, China
[c] Shandong Provincial NO.4 Institute of Geological and Mineral Survey, Weifang 261021, China
[d] Department of Earth and Environmental Sciences, Michigan State University, East Lansing, MI 48824, USA
[e] State Key Laboratory of Ore Deposit Geochemistry, Institute of Geochemistry, Chinese Academy of Sciences, Guiyang 550081, China

ARTICLE INFO

*Keywords:*
Crustal growth
Oceanic plateau
Amdo microcontinent
Bangong-Nujiang suture zone
Central Tibetan Plateau

ABSTRACT

The oceanic lithosphere subduction has been attested to exert the first-order control on the formation of the continental crust, but the role of oceanic plateaus on the crustal growth is elusive. It is difficult to identify the component of the oceanic plateaus in the continental crust because of their disappearance after subduction into deep mantle or obduction to be a part of the ophiolite mélanges in the ancient orogenic belts. Amdo microcontinent in the central Tibetan Plateau is an ideal place to assess the role of oceanic plateaus on crustal growth as it preserves the well-exposed arc magmatic rocks and fragments of the Meso-Tethyan oceanic plateaus to its south. Here, we present an integrated investigation of zircon U—Pb ages and Hf isotope, as well as whole-rock elements and Sr-Nd-Hf isotopes of a suit of dacites in the Amdo microcontinent. Zircon U—Pb dating indicates that the Amdo dacites formed at ca. 117 Ma, postdated the major formation period of the Meso-Tethyan oceanic plateaus. The Amdo dacites have relatively high $SiO_2$ (63.45–66.82 wt%) contents and low Mg# values (20.0–36.1), belonging to calc-alkaline series. The zircon thermometer and oxybarometer give estimated temperature and oxygen fugacity of crystallization as ca. 700–720 °C and ΔFMQ = + 0.98, respectively. The Amdo dacites have low Y (5.51–6.61 ppm) and Yb (0.44–0.53 ppm) contents and high La/Yb ratios (28.4–30.3). Despite their low Sr/Y ratios (6.86–13.5) caused by a small degree of fractionation of plagioclase, the Amdo dacites have an adakitic geochemical affinity, which was most likely derived from the thickened continental lower crust. These dacites have more depleted Sr-Nd-Hf isotope compositions (whole-rock $^{87}Sr/^{86}Sr_i$ = 0.709796–0.710563, $\varepsilon_{Nd}(t)$ = −3.27 to −2.82, $\varepsilon_{Hf}(t)$ = 4.20–4.83 and zircon $\varepsilon_{Hf}(t)$ = 4.2–8.8) than the Neoproterozoic and Cambrian orthogneisses, as well as the Jurassic magmatic rocks. Simple binary mixing modeling reveals that the Amdo dacites could represent the hybrid melts of 50–60% of the subducted Meso-Tethyan oceanic plateau materials with 50–40% of the Amdo ancient continental crustal materials. The decoupled whole-rock Nd—Hf isotopes ($\Delta\varepsilon_{Hf}(t)$ = 7.55–8.43) of the Amdo dacites could be explained by the addition of zircon-free sediments overlie on the oceanic plateaus. These results indicate that subduction of the Meso-Tethyan oceanic plateaus with/without the overlying sediments have made a substantial contribution to continental crustal growth. In conjunction with previous studies, we conclude that the subduction of the Meso-Tethyan oceanic plateaus may have intermittently occurred for around 37 million years, thus highlighting the significance of subduction of the Meso-Tethyan oceanic plateaus during the secular evolution of the central Tibetan Plateau.

* Corresponding author at: 29 Xueyuan Road, Haidian District, Beijing 100083, China.
*E-mail address:* fenghuang@cugb.edu.cn (F. Huang).
[1] Joint first author.

https://doi.org/10.1016/j.lithos.2022.106944
Received 22 August 2022; Received in revised form 8 November 2022; Accepted 8 November 2022
Available online 13 November 2022

## 1. Introduction

The continental crust on the Earth is a unique component in our solar system that contains the secular rocks and minerals since the Hadean eon (Rudnick and Gao, 2014). Ascertaining its generation and evolution holds the key to understanding the differentiation of the silicate planet and its habitability. As the continental crust and arc magmas share similar trace-element characteristics (Rudnick and Gao, 2014), it is generally believed that oceanic arc system is the most important site of juvenile continental crust formation as long as plate tectonics has operated (Condie and Kröner, 2013; Hu et al., 2021a; Wang et al., 2021a). Traditionally, the arc magmas were thought to be generated from mantle wedge fluxed by the fluids released from the subducted slab (e. g., Stern, 2020). However, it continuously arises controversy on what roles of other components of the oceanic slab played in the continental crustal growth. For example, oceanic plateaus are widely distributed in the modern and ancient oceans (e. g., Lu et al., 2016), and the amalgamation of oceanic plateaus and continental fragments has been suggested to be an effective way to form large segments of the continental crust (e. g., Vogt and Gerya, 2014). On the other hand, the subduction of the oceanic plateaus in an arc system also has the potential to facilitate crustal growth by flat subduction or relamination, due to their lower density than the ambient mantle (Gutscher et al., 2000; Ji et al., 2021). Therefore, the influence of subduction of the oceanic plateaus on continental crustal growth needs to be assessed.

The Tibet-Himalaya orogenic belt is a typical collision orogeny belt, formed by the closure of several Tethys oceans with variable ages and continental collision (Hu et al., 2021b; Zhu et al., 2011; Zhu et al., 2013). The Bangong-Nujiang suture (BNS) separates Lhasa and Qiangtang Terranes and is preserved within the central Tibetan Plateau, representing relicts of the Bangong-Nujiang Ocean (also called Meso-Tethyan ocean; Wang et al., 2016; Zhu et al., 2016). Arc-related magmatic rocks with crystallization time of Middle Jurassic to Early Cretaceous were widely developed on both sides of the BNS, revealing processes associated with subduction of the oceanic lithosphere (e. g., Hu et al., 2022; Li et al., 2020a; Zhu et al., 2016). In the interior of the

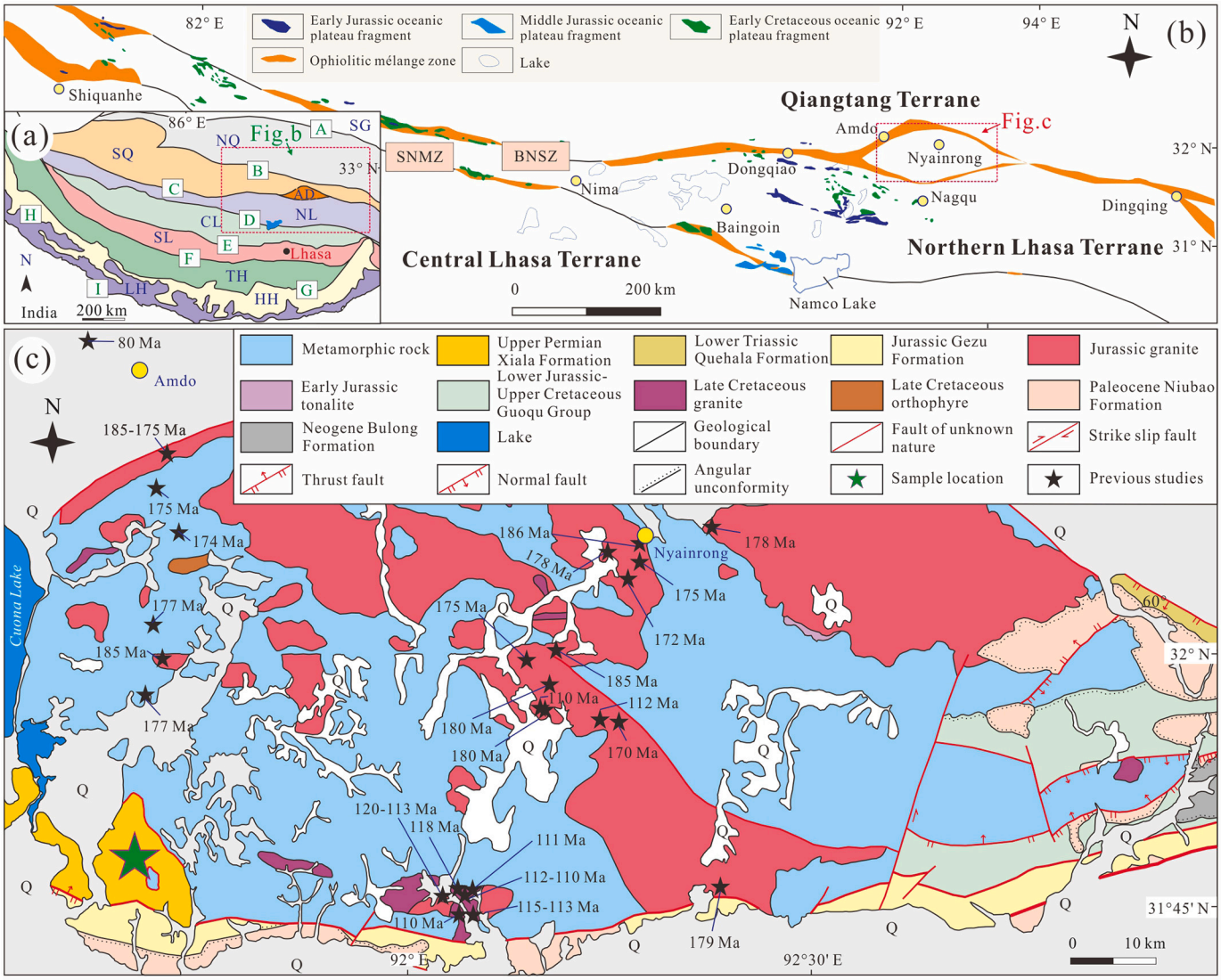


**Fig. 1.** (a) Tectonic framework of the Tibetan Plateau. (b) Geological sketch maps of the ophiolite mélange zone and fragments of the oceanic plateaus in the central Tibetan Plateau. (c) Geological map of the Amdo microcontinent showing sample location. Abbreviations: SG-Songpan-Ganzi Terrane; NQ-Northern Qiangtang Terrane; SQ-Southern Qiangtang Terrane; AD-Amdo microcontinent; NL-northern Lhasa Terrane; CL-central Lhasa Terrane; SL-southern Lhasa Terrane; TH-Tethyan Himalayae; HH-High Himalaya; LH-Lesser Himalaya; A-Jinsha suture zone; B-Longmuco–Shuanghu suture zone; C-Bangong-Nujiang suture zone (BNSZ); D-Shiquanhe-Namco mélange zone (SNMZ); E-Luobadui-Milashan fault; F-Indus-Yarlung Zangbo suture zone; G-South Tibetan detachment system; H-Main boundary thrust; I-Main boundary thrust. The maps are modified from Wu et al. (2022) and Zhang et al. (2014).

suture zone, some oceanic island basalt (OIB)-type pillow igneous rocks interbreed with limestone distributed extensively (e. g., Fan et al., 2021), which represent remnants of the missing Meso-Tethyan oceanic plateaus (Zhang et al., 2014). The Meso-Tethyan oceanic plateaus erupted at peaking timing of the Early Jurassic (~185 Ma) and Early Cretaceous (~ 121 Ma), with the remnants covering an area of $>2 \times 10^5$ $km^2$ in the central Tibetan-Plateau along the Bangong-Nujiang suture zone (Fig. 1a; Zhang et al., 2014). Recent studies have demonstrated that these oceanic plateaus make critical contributions not only to the magmatic rhythm of the active continental margin, but also to the tectonic evolution of the central Tibetan Plateau. For instance, the collision between the Meso-Tethyan oceanic plateaus and Qiangtang Terrane resulted in a magmatic lull and subsequent magmatic arc jumping, with the arc-type magmatic rocks replaced by OIB-type rocks (Zeng et al., 2021; Zhang et al., 2021). The wholesale obduction of the Meso-Tethyan oceanic plateaus over the Tibetan continental crust could have given rise to approximately 2 km elevation of the central Tibetan Plateau following the final closure of the Bangong-Nujiang Ocean (Zhang et al., 2014). The relamination of the Meso-Tethyan oceanic plateaus after the oceanic demise might also lead to vertical continental growth on the continental margin (Ji et al., 2021). However, it is still unclear whether the Meso-Tethyan oceanic plateaus have exerted significant control on the crustal growth during the subduction of the Bangong-Nujiang oceanic plate.

The Amdo microcontinent with a Precambrian crustal basement, is located at the central part of the Bangong-Nujiang suture zone (Fig. 1). To its immediately south, the tectonic property of Beila-Nagqu ophiolitic mélange is still controversial, including a complex arc-trench system (Li et al., 2020a) or a microcontinent (Hu et al., 2022). A recent study of Zhang et al. (2021) shows that the Pengco cumulates in the Beila-Nagqu ophiolitic mélange were genetically related to mantle plume activity, representing the lower crust of a Jurassic oceanic plateau. They further proposed that the oceanic plateau-Qiangtang collision and arc magmatism jump the south (Zhang et al., 2021). Except the obduction relicts overlie on the surface, the other section of the oceanic plateau might subduct northwards. It is reasonable to speculate that there was a branch of the Bangong-Nujiang Ocean with an oceanic plateau to the south of the Amdo microcontinent. The oceanic plateau, coupled with the oceanic lithosphere likely subducted beneath the Amdo microcontinent. Therefore, the Amdo microcontinent provides an optimal place to address how the likely oceanic plateau subduction contributes to crustal growth since the juvenile crustal materials could be easily identified via the junctional whole-rock element and radiogenic Sr-Nd-Hf isotope compositions.

In this contribution, we report zircon U—Pb geochronological, trace elemental, and Hf isotopic data, as well as the whole-rock elemental and Sr-Nd-Hf isotopic data of newly found dacite samples in the Amdo microcontinent, central Tibetan Plateau. These new data indicate that the Amdo dacites formed in the Early Cretaceous (ca. 117 Ma) showing adakitic geochemical affinity. The Sr-Nd-Hf isotopes reveal that the Amdo dacites were derived from a thickened continental lower crust by subduction and underplating of the Meso-Tethyan oceanic plateaus. In conjunction with previous studies, we propose that the subduction of the Meso-Tethyan oceanic plateaus is a very likely mechanism for crustal growth in the convergent continental margin, in spite that the actual growing amount needs further estimate.

## 2. Geological background and sample descriptions

The Tibet-Himalaya orogenic belt is a result of the drift and amalgamation of several continents and microcontinents from the Gondwana supercontinent. It consists of the Songpan–Ganzi flysch complex, the Qiangtang, Lhasa, and Himalayas Terranes from north to south (Fig. 1a; Hu et al., 2021b; Zhu et al., 2013; Wang et al., 2021b; Zhu et al., 2011). The BNS in the central Tibetan Plateau between the Lhasa and Qiangtang Terranes is generally thought to represent relicts of a Bangong-Nujiang Ocean, the timing of the ophiolites in the Bangong-Nujiang suture zone is mainly in Early–Middle Jurassic (e. g., Liu et al., 2022; Wang et al., 2016). Previous studies suggested that the Bangong-Nujiang Ocean completely closed during the Late Mesozoic (e.g., Peng et al., 2020; Zhu et al., 2016). Although the opening time of the Bangong-Nujiang Ocean is still unclear, Meso-Tethyan oceanic plateaus with age of Early Jurassic-Early Cretaceous have been identified in the Bangong-Nujiang Ocean by Zhang et al. (2014). These oceanic plateaus were represented by the ophiolite relics scattered between the towns of Shiquanhe and Naqu along the Bangong-Nujiang suture zone (Fig. 1b).

Within the middle sector of the Bangong-Nujiang suture zone, the Amdo (or Nyainrong) microcontinent wrapped by ophiolites is well exposed (Fig. 1b;Guynn et al., 2006; Xie, 2013; Zhang et al., 2012). The Amdo microcontinent is in fault contact with Mesozoic sedimentary rocks in the Lhasa and Qiangtang Terranes (Fig. 1c; Xie, 2013). The Amdo microcontinent is composed of a basement metamorphic complex, undeformed granitoids, and minor Paleozoic–Cenozoic strata (Fig. 1c). The metamorphic complex consists of amphibolite- to greenschist-facies orthogneisses and subordinate metasedimentary rocks overlain by Paleozoic–Cenozoic strata (Li et al., 2017). The protoliths of the orthogneisses are mostly granite and granodiorite with subordinate monzonite, tonalite, and quartz-diorite (Guynn et al., 2012) with ages of 661–820 Ma (Dong et al., 2011; Liu et al., 2021; Yu et al., 2021). Occasionally, Neoproterozoic orthogneiss with intense deformation and migmatization occurs as inclusions within the early Paleozoic orthogneiss (Liu et al., 2021). The early Paleozoic orthogneisses show crystallization ages of ca. 483–532 Ma, suggesting that the Amdo microcontinent may have experienced Pan–African orogeny (Guynn et al., 2006; Xie, 2013; Zhang et al., 2012). The Mesozoic magmatic rocks are well-developed and dominated by Early–Middle Jurassic granitoids accompanied by some Cretaceous granitoids, which intruded into the metamorphic complex (Fig. 1c; Guynn et al., 2006; Liu, 2012; Xie, 2013; Yan et al., 2016). Extensive Early Jurassic metamorphism (e. g., eclogite and granulite) has also been documented in the Amdo microcontinent (Guynn et al., 2006; Peng et al., 2022; Zhang et al., 2012). The volumetrically minor clastic rocks of Cenozoic Niubao formation are distributed sporadically in the east of the microcontinent.

The dacite samples in this study (hereafter Amdo dacites) were collected in the southwest of the Amdo microcontinent, ca. 80 km south of Amdo town (Fig. 1c). The Amdo dacites occur as extended dikes with associated flows, which intruded into the limestone of Permian Xiala Formation (Figs. 1c and 2). No chilled border or metasomatic minerals on the boundary of the silicate and carbonate rocks have been found. Most of the sampled dikes display an east-to-west trend with a width of 0.3–1 m and a length of 1 m to >10 m. All the Amdo dacite samples experienced variable degrees of alteration. They display porphyritic texture with phenocryst phases of 15–25 vol% plagioclase (0.3–2 mm in length) and 10–20 vol% quartz (0.2–0.5 mm in length), and the groundmass mainly consists of microlitic felsic minerals (Fig. 2).

## 3. Results

Zircon U—Pb dating and trace element analyses were performed at Guangxi Key Laboratory of Hidden Metallic Ore Deposits Exploration, Guilin University of Technology (GUT), Guilin, China. Whole-rock major and trace elemental composition was analyzed at the Wuhan Sample Solution Analytical Technology Co., Ltd., Wuhan, China. Chemical separation of whole-rock Sr-Nd-Hf isotopes were conducted at the GUT, and measurement of Nd—Hf and Sr isotopic compositions were performed at the GUT and State Key Laboratory of Ore Deposit Geochemistry, Institute of Geochemistry, Chinese Academy of Sciences, respectively. Detailed analytical procedures are given in the supplementary materials. Laser ablation inductively coupled plasma mass spectrometry (LA–ICP–MS) zircon U—Pb geochronology, trace elements compositions, whole rock major and trace element, Sr-Nd-Hf isotope, and zircon Hf isotope data for the Amdo dacites are given in supplementary Tables S1–S5.

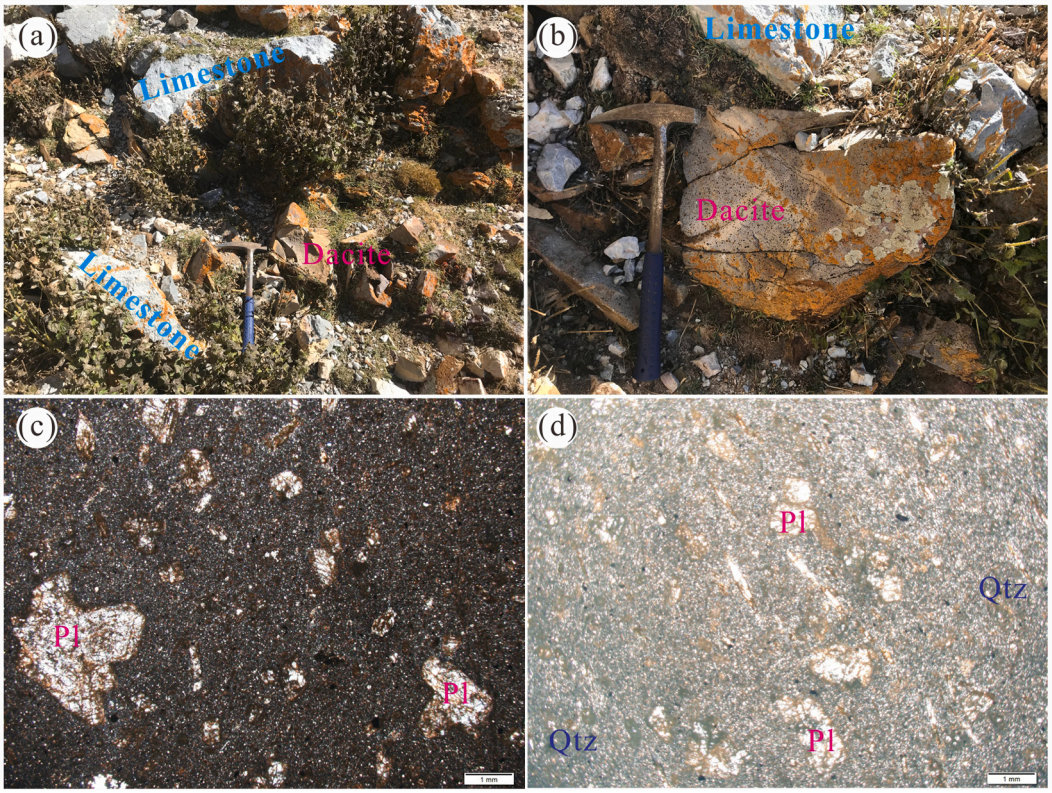


**Fig. 2.** (a-b) Photograph of the outcrops of the Amdo dacites. (c-d) Photomicrographs (in cross-polarized light) of the Amdo dacites. Abbreviations: Pl-plagioclase, Qtz-quartz.

### 3.1. Zircon geochronology and trace elements

Zircon grains of Amdo dacites are all transparent and elongate, about 30–150 μm long with aspect ratios of 1.5:1–3:1 (Fig. 3a). Cathodoluminescence (CL) images of the zircon grains show a narrow rim of concentric oscillatory zoning with variable brightness, which is commonly observed in zircons from acidic magmas (Corfu et al., 2003). All the zircons have Th/U ratios ranging from 0.31 to 0.95 (Table S1), and show strong positive Ce anomalies, negative Eu anomalies, and enrichment in heavy rare earth elements (HREEs) in chondrite-normalized REE patterns (Fig. 3b, Table S2). They show a distinct affinity with those from continental zircons globally (Figs. 3c, d; Grimes et al., 2009). All the above characteristics suggest that the zircons have a magmatic origin. 15 analyses of 18 zircon grains yielded a weighted mean $^{206}Pb/^{238}U$ age of 117.2 ± 0.8 Ma (MSWD = 1.0; Fig. 3a). Other three zircon grains yielded ages of 552, 438 and 163 Ma (Fig. 3a), which are comparable to the timing of Gondwana assembly and Bangong-Nujiang Oceanic plate subduction (Guynn et al., 2012; Xie, 2013; Yan et al., 2016; Zhang et al., 2012), thus representing inherited zircons in the dacites. The inherited zircons show distinctly lower Yb contents than the Cretaceous magmatic zircons (Fig. 3b).

### 3.2. Whole-rock major and trace elements

The investigated volcanic samples stretch across the fields of subalkaline dacite to trachyandesite on a Nb/Y vs. $Zr/TiO_2 \times 0.0001$ diagram (Fig. 4a), and in the field of calc-alkaline dacite on a Th—Co diagram (Fig. 4b). They have a relatively homogeneous geochemical composition with high $SiO_2$ (63.45–66.82 wt%), $Al_2O_3$ (13.51–14.40 wt%), CaO (6.80–8.66 wt%) contents, low MgO (0.12–0.18 wt%) and $TiO_2$ (0.26–0.29 wt%) contents. The Mg# (= $100 \times Mg^{2+}/(Mg^{2+} + Fe^{2+})$) of the Amdo dacites range from 20.0 to 36.1, which are comparable with the lower crust-derived melts (Rapp and Watson, 1995). Accordingly, the volcanic rocks in this study belong to calc-alkaline dacite.

The Amdo dacite samples exhibit low concentrations of compatible trace elements, such as Cr (10.79–11.46 ppm) and Ni (4.62–8.58 ppm). In a chondrite-normalized REE diagram, they show the largest light and heavy REE fractionation among the present orthometamorphic and magmatic rocks in the Amdo microcontinent with ages ranging from Neoproterozoic to Cretaceous (Fig. 5a). The Amdo dacite samples have high La/Yb ratios (28.4–30.3) and low Yb contents (0.44–0.53 ppm; Table S3). Contrary to the ubiquitous strong negative Eu anomalies in Neoproterozoic and Cambrian orthogneisses and Jurassic magmatic rocks in the Amdo microcontinent (Hu et al., 2021b; Li et al., 2017; Liu, 2012; Liu et al., 2017; Liu et al., 2021; Lu et al., 2014; Xie, 2013; Yan et al., 2016; Yu et al., 2021; Zhu et al., 2011), our Cretaceous Amdo dacites show limited negative Eu anomalies (δEu = 0.85–0.99; $\delta Eu = Eu_N/(Sm_N \times Gd_N)^{0.5}$, the subscript N represents chondrite-normalized), which is comparable to the coeval magmatism (Fig. 5a; Ji et al., 2021; Zhu et al., 2011). In a primitive mantle (PM)-normalized multi-element diagram (Fig. 5b), the samples are typified by enrichment in Th, U and light REEs, relative to high field strength elements (HFSEs) such as Nb and Ta. They also have low concentrations of mobile elements (e. g., Rb, Ba and Sr), resulting in low Sr/Y ratios (6.86–13.5).

### 3.3. Whole-rock Sr-Nd-Hf isotopes

The initial $^{87}Sr/^{86}Sr$, $^{143}Nd/^{144}Nd$ and $^{176}Hf/^{177}Hf$ ratios of the Amdo dacite samples were calculated based on the zircon U—Pb age of 117 Ma. The analyzed samples show radiogenic Sr ($^{87}Sr/^{86}Sr_i$ = 0.709796–0.710563) and unradiogenic Nd ($^{143}Nd/^{144}Nd_i$ = 0.512320–0.512343), corresponding to $\varepsilon_{Nd}(t)$ values of −3.27 to −2.82 (Fig. 6a). The Sr—Nd isotope compositions of the dacites in the present study are more depleted than most of Neoproterozoic and Cambrian orthogneisses and Jurassic magmatic rocks in the Amdo microcontinent (Harris et al., 1988; Hu et al., 2021b; Li et al., 2017; Liu, 2012; Liu et al.,

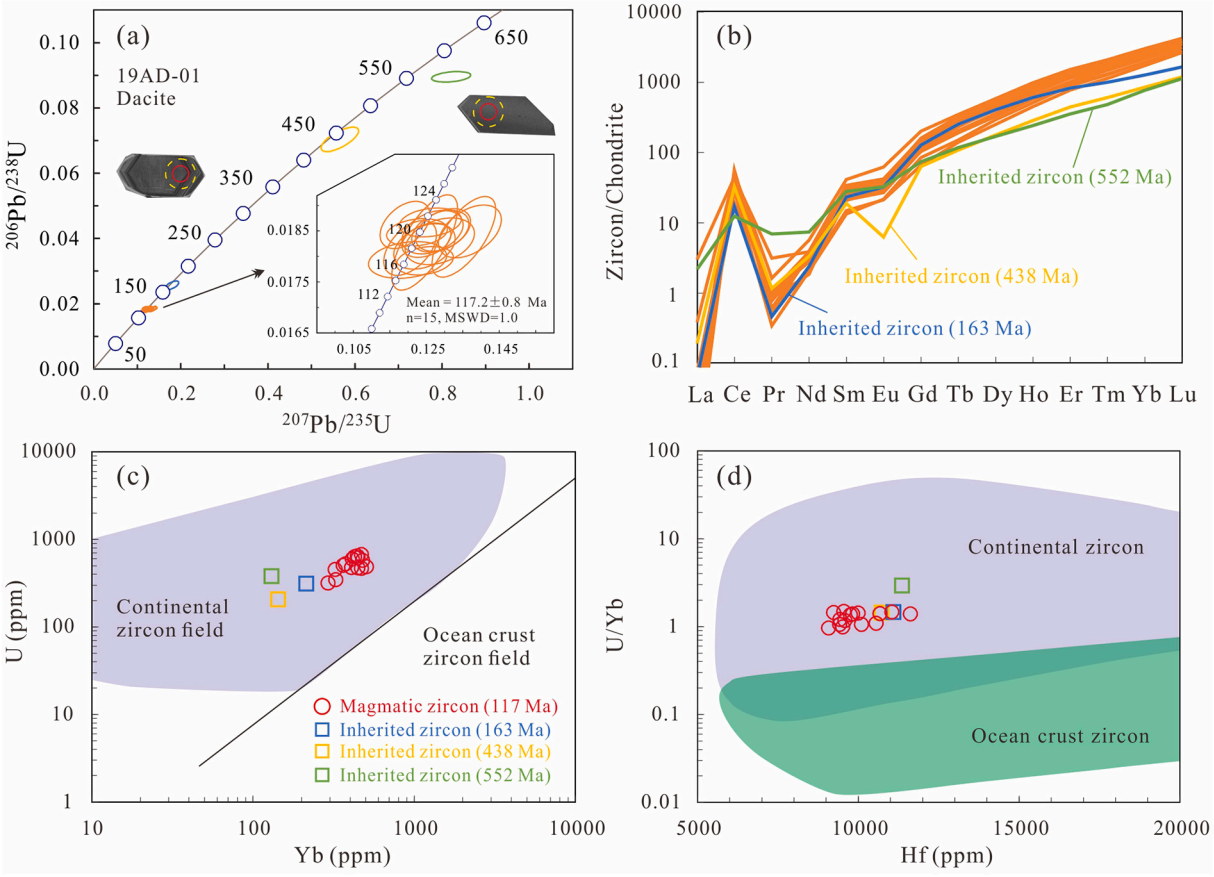


**Fig. 3.** (a) Zircon LA–ICP–MS U—Pb concordia and weighted mean age of the analyzed zircons for the represent Amdo dacite sample (19AD-01). (b) Chondrite-normalized REE patterns of the zircons (normalized values are from Sun and McDonough, 1989). (c) U versus Yb and (d) U/Yb versus Hf variation diagrams for magmatic zircons from different sources (Grimes et al., 2009).

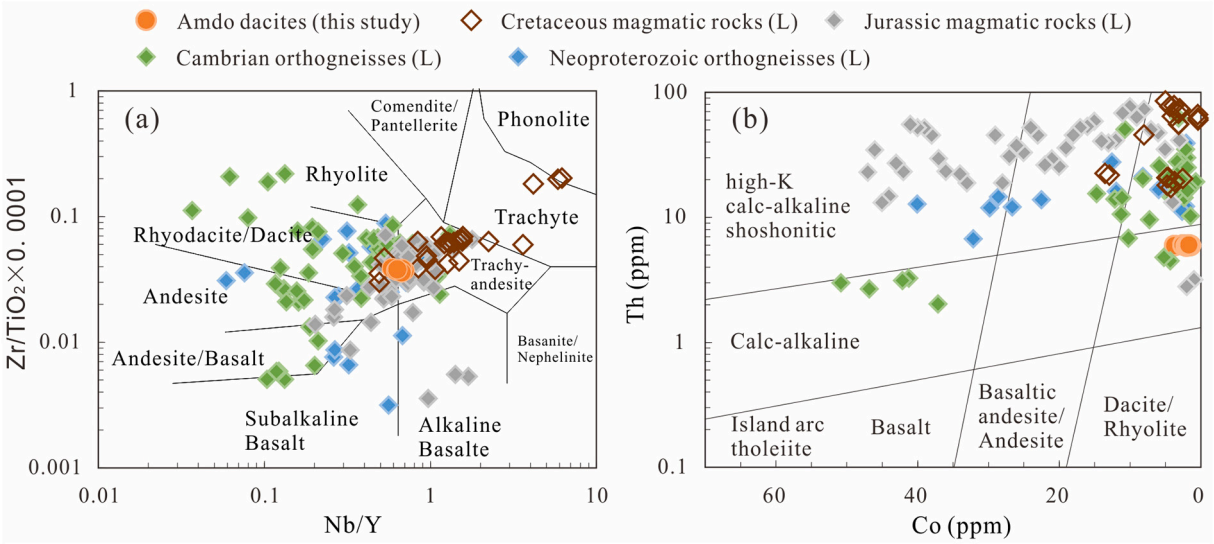


**Fig. 4.** (a) $Zr/TiO_2 \times 0.0001$ versus Nb/Y diagram and (b) Th versus Co diagram. Data sources: Cretaceous magmatic rocks are from Liu et al. (2017), Wu et al. (2022), and Zhu et al. (2011); Jurassic magmatic rocks are from Li et al. (2017), Liu (2012), Liu et al. (2017), Liu et al. (2022), Zhu et al. (2011) and Yan et al. (2016); Cambrian orthogneisses are from: Harris et al. (1988), Hu et al. (2021b), Lu et al. (2014), Xie (2013) and Zhang et al. (2012); Neoproterozoic orthogneisses are from: Liu et al. (2021), Xie (2013), Yu et al. (2021) and Zhang et al. (2012). Abbreviation: L-literature.

2021; Liu et al., 2022; Lu et al., 2014; Xie, 2013; Yan et al., 2016), except a few Jurassic magmatic rocks with depleted Sr—Nd isotope composition which were likely hybrid melts between the asthenosphere and lithospheric mantle (Liu, 2012; Yan et al., 2016). Likewise, the Amdo dacites show more depleted Nd isotope compositions than the Cretaceous granitoids (Fig. 6a; Liu et al., 2017; Wu et al., 2022). The two-

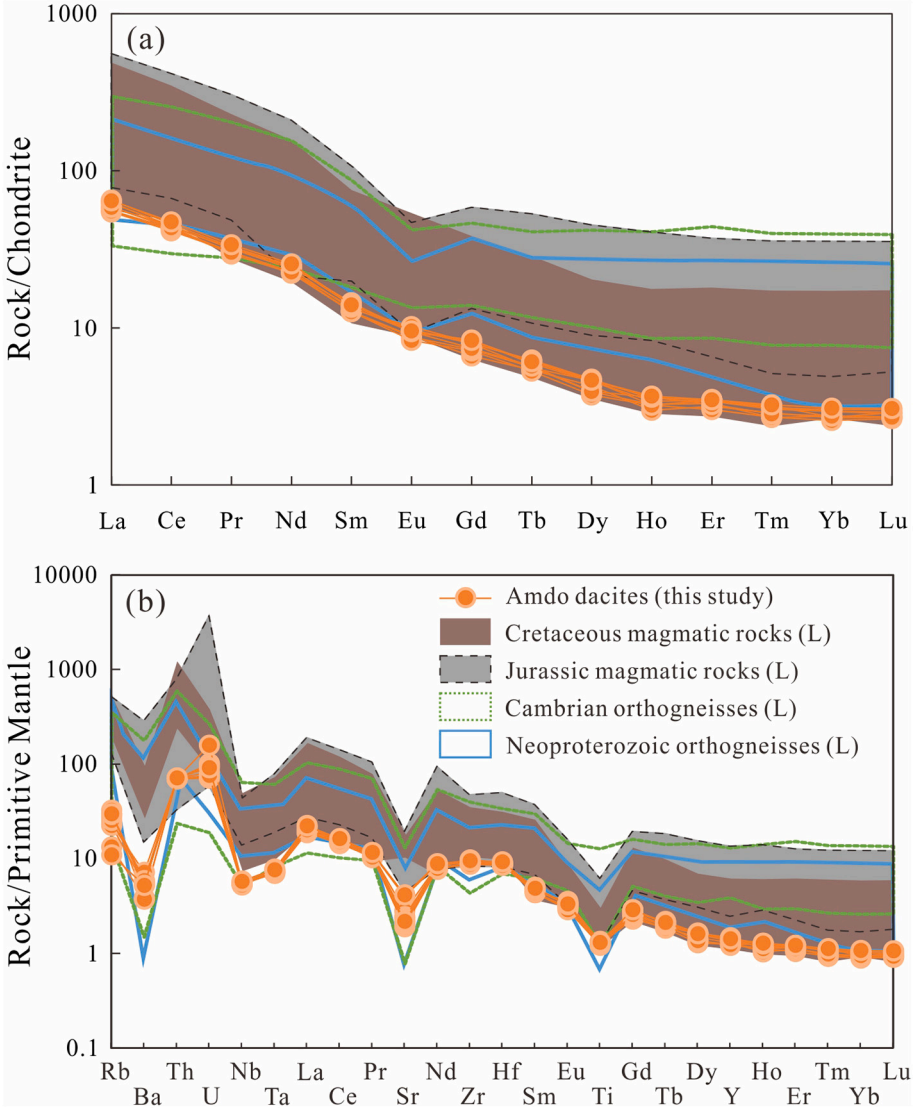


**Fig. 5.** (a) Chondrite-normalized REE patterns and (b) primitive mantle-normalized multi-element diagrams for the Amdo dacite samples. The Neoproterozoic and Cambrian orthogneisses and Jurassic magmatic rocks in the Amdo microcontinent are also shown for comparison. The chondrite and primitive mantle values are from Sun and McDonough (1989). The data sources are same as in Fig. 4.

stage Nd isotope model ages ($T^2_{DM}$, based on the continental crust) of the Amdo dacites are ranging from 1.14 to 1.18 Ga (Table S4).

The Amdo dacites have low $^{176}Lu/^{177}Hf$ (0.003–0.004) and high $^{176}Hf/^{177}Hf_i$ (0.282237–0.282312), corresponding to $\varepsilon_{Hf}(t)$ values of 4.20 to 4.83. As no whole-rock Hf isotope data have been reported in the literature, we compare the whole-rock $\varepsilon_{Hf}(t)$ with the zircon $\varepsilon_{Hf}(t)$ in the previous studies. These dacites have much higher $\varepsilon_{Hf}(t)$ values compared with the igneous rocks with varied ages in the Amdo microcontinent (Fig. 6b; Hu et al., 2021b; Liu, 2012; Wu et al., 2022). The Hf isotope crustal model ages ($T^2_{DM}$) of the Amdo dacites range from 864 to 904 Ma (Table S4). The Amdo dacite samples have high $\varepsilon_{Hf}(t)$ at a given $\varepsilon_{Nd}(t)$ compared to the $\varepsilon_{Nd}(t)$–$\varepsilon_{Hf}(t)$ terrestrial array (Fig. 6b) with $\Delta\varepsilon_{Hf}(t)$ ranging from 7.55 to 8.43 (Table S4) ($\Delta\varepsilon_{Hf}$ is defined as the deviation of $\varepsilon_{Hf}$ from the global terrestrial array, $\Delta\varepsilon_{Hf} = \varepsilon_{Hf} - 1.55 \times \varepsilon_{Nd}$-1.21; Vervoort et al., 2011), which is also apparently different to other magmatic rocks in Amdo microcontinent.

### 3.4. Zircon Hf isotopes

Zircons from the dacite sample 19AD-01 show a range of initial $^{176}Hf/^{177}Hf$ ratios from 0.282817 to 0.282946 and $\varepsilon_{Hf}(t)$ values ranging from 4.2 to 8.8, with Hf isotope crustal model ages ($T^2_{DM}$) of 614 to 905 Ma (Fig. 6c). The lower limit of the zircon $\varepsilon_{Hf}(t)$ in Amdo dacites is comparable with the whole-rock $\varepsilon_{Hf}(t)$. The present dacites show the highest $\varepsilon_{Hf}(t)$ values among the published Amdo orthometamorphic and magmatic rocks (Fig. 6c; Hu et al., 2021b; Li et al., 2017; Liu, 2012; Liu et al., 2021; Lu et al., 2014; Wu et al., 2022; Xie, 2013; Zhu et al., 2011). The inherited zircon grains show much lower $\varepsilon_{Hf}(t)$ values of −15.5 (163 Ma) and − 21.6 (438 Ma) than the main cluster (Fig. 6d), and they have Hf isotope crustal model ages of 2.19–2.77 Ga (Table S5).

## 4. Discussion

### 4.1. Magma temperature and oxygen fugacity

In the felsic magmatic system, zircon saturation is mainly controlled by the magma composition and temperature. Accordingly, a whole-rock zircon saturation thermometer first proposed by Watson and Harrison (1983) and updated by Boehnke et al. (2013) could be used to estimate the temperature of the solidus. Using the updated thermometer, the whole-rock zircon saturation temperature of the Amdo dacites is 680–713 °C (mean 702 ± 12 °C; Fig. 7; Table S3). The temperature of

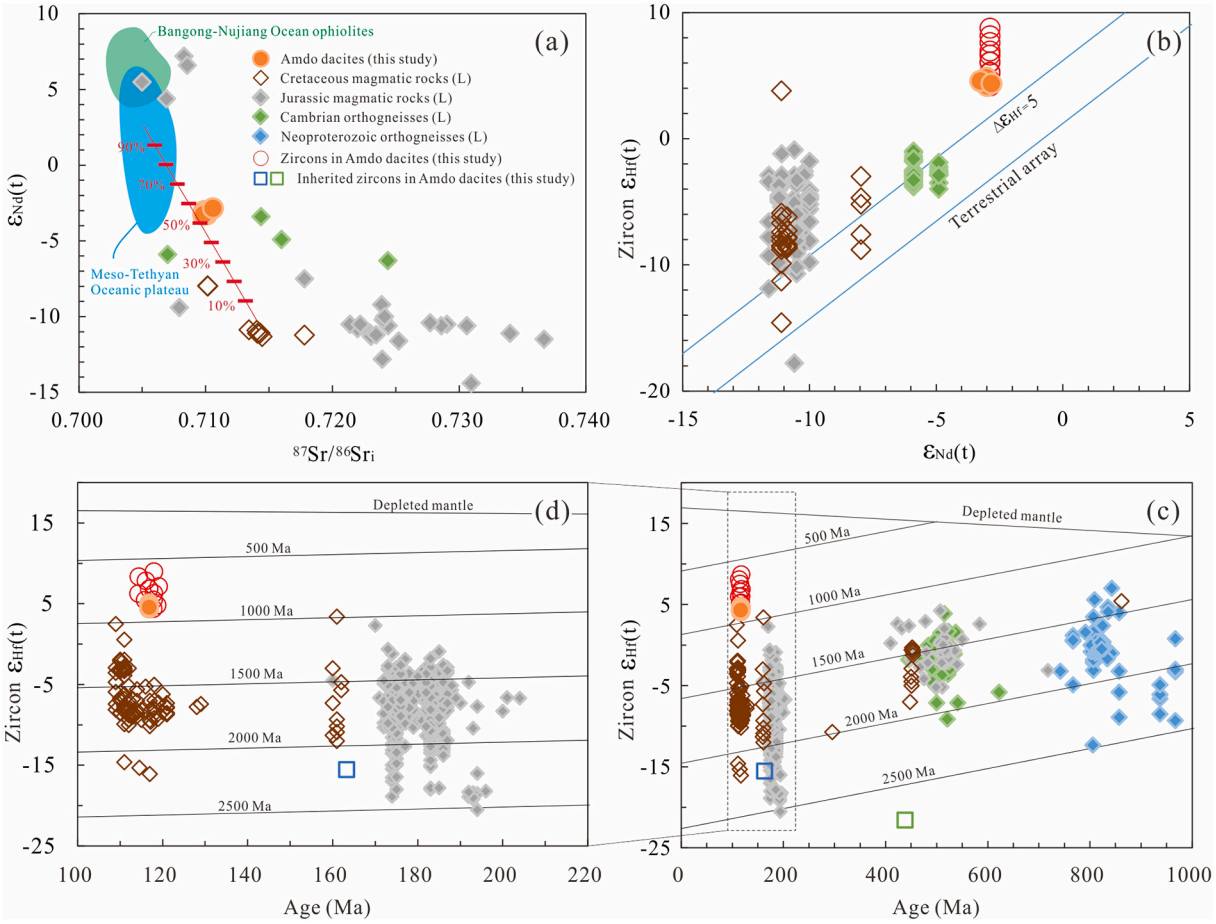


**Fig. 6.** (a) $^{87}Sr/^{86}Sr_i$ versus $\varepsilon_{Nd}(t)$ diagram, (b) whole-rock $\varepsilon_{Nd}(t)$ versus zircon $\varepsilon_{Hf}(t)$ diagram, and (c-d) plots of U—Pb ages versus zircon $\varepsilon_{Hf}(t)$ of the Amdo dacite samples. The data of Neoproterozoic and Cambrian orthogneisses, Jurassic magmatic rocks, and their contained zircons in the Amdo microcontinent are also shown for comparison. During the binary mixing model, the average values of the Sr—Nd isotope compositions Meso-Tethyan oceanic plateaus and the Cretaceous granitoids were used, we also assumed that the melts of oceanic plateau materials and the Amdo crustal basement have the same Sr and Nd concentrations with Sr = 150 ppm and Nd = 10 ppm. The data sources for the orthogneisses and magmatic rocks are same as Fig. 4. The data for the Bangong-Nujiang ocean ophiolites are from Wang et al. (2016) and reference therein. The data for the Meso-Tethyan oceanic plateaus are from Zhang et al. (2014).

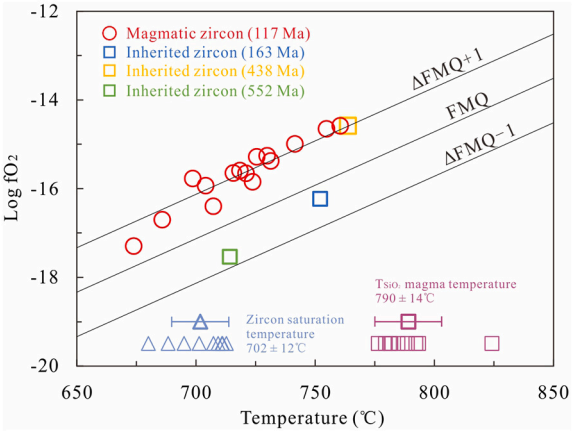


**Fig. 7.** Temperature versus Logf$O_2$ diagram for the Amdo dacites. The temperature in the x-coordinate is represented by the Ti-in-zircon temperature (Ferry and Watson, 2007), and the oxygen fugacity is calculated referring to Loucks et al. (2020). The whole-rock zircon saturation temperature (Boehnke et al., 2013) and Tsio$_2$ magma temperature (Duan et al., 2022) are also shown for comparison.

680–713 °C should principally represent the actual crystallization temperature of magma due to the presence of old inherited zircons.

Whole-rock $SiO_2$ is an essential constituent of granitoid rocks and magmas, and $SiO_2 \propto 1/T$ is constrained by experimental phase equilibria, $SiO_2$ content could be used as a proxy to estimate granitoid magma temperatures. Recently, new thermometry called $T_{SiO2}$ was developed by Duan et al. (2022) to calculate the felsic magma temperature. The calculated magma temperature of the Amdo dacites is 777–825 °C (mean 790 ± 14 °C; Fig. 7; Table S3). This temperature is much higher than the zircon saturation temperatures, which could be a result of the lower measured values than the actual $SiO_2$ contents of the Amdo dacites, because the samples in this study have a relatively high loss on ignition (LOI; ~10 wt%; Table S3).

Titanium content of zircon coexisting with rutile and the Zr content of rutile coexisting with zircon has a strong temperature dependence, the magma temperature could be estimated by a Ti-in-zircon geothermometer at given $SiO_2$ and $TiO_2$ activities (Ferry and Watson, 2007). Since no rutile was found in the samples, the $TiO_2$ activity ($\alpha TiO_2$) and $SiO_2$ activity ($\alpha SiO_2$) were assumed to be 0.7 and 1, respectively. Our calculation results show that the Ti-in-Zircon temperature is 674–761 °C (mean 719 ± 24 °C; Fig. 7; Table S3), which is close to the zircon saturation temperature. Accordingly, we proposed that the liquidus temperature of the Amdo dacites is ca. 700–720 °C.

Trace elemental compositions in the zircons depend not only on the magma temperature but the oxidation state. Without an independent

determination of crystallization temperature or pressure or parental melt composition, Loucks et al. (2020) developed a new magmatic oxybarometer using ratios of Ce, U, and Ti in zircon. It yields results in good agreement with oxybarometry on mineral phenocrysts in eruptive dacites and rhyolites. Estimated by this new oxybarometer, the Amdo dacites show moderately oxidized with ΔFMQ = +0.54 − +1.40 (mean + 0.98 ± 0.24; FMQ represents the reference buffer fayalite + magnetite +quartz) (Fig. 7), which is similar to the Phanerozoic arc magmas (ΔFMQ ≈ +1 to +2; Richards, 2022). Except for the inherited zircon with 438 Ma shows a comparable oxygen fugacity with the Cretaceous zircons, the other two inherited zircons (163 Ma and 552 Ma) show more reduced (ΔFMQ = −0.40 and − 0.77; Table S2). Therefore, the Amdo dacites formed at a relatively low temperature and moderately oxidized environment.

### 4.2. Alteration, shallow crustal contamination, and fractional crystallization

#### 4.2.1. Degassing, low-grade metamorphism and weathering

The Amdo dacites are surrounded by limestone of the Permian Xiala Formation (Fig. 1), which may promote the capture of calcite ($CaCO_3$) and release of carbon dioxide, and then change the composition of the whole rocks. The dacites in this study have relatively high LOIs (Table S3) and oceanic carbonate-like Sr isotopic composition ($^{87}Sr/^{86}Sr \approx 0.709$, Fietzke et al., 2008), which seems to be consistent with the carbonate contamination and subsequent $CO_2$ degassing processes. However, these dacites also show two orders of magnitude lower Sr concentrations (40.1–87.1 ppm) than the carbonate (>1000 ppm; Fietzke et al., 2008), in disagreement with the capture of a small volume of calcites.

Such a high LOIs (up to 12 wt%) and low contents (<0.5 wt%) of mobile alkaline metal oxides (i. e., $Na_2O$ and $K_2O$) of the Amdo dacites may indicate that they might have undergone low-grade metamorphism or variable degrees of weathering. The potential effects of these processes on their chemical compositions should be evaluated. Given that Zr is a highly immobile element during low-grade metamorphism and post-magmatic alteration, it can be used to discriminate the mobility of other elements (e.g., Huang et al., 2021b). As shown in Fig. 8, Rb and Ba are negatively correlated with Zr in the Amdo dacites, suggesting they were mobile during the post-magmatic processes; whereas the other fluid-mobile element Sr shows a strong positive correlation with Zr, which indicates Sr is immobile. Thus, the initial Sr isotope calculated by the formation age and the $^{87}Rb/^{86}Sr$ ratios should be lower than the actual $^{87}Sr/^{86}Sr_i$ values of the Amdo dacites.

Other incompatible elements such as Th (Fig. 8d), high field-strength elements (HFSEs, represented by Figs. 8d and i), REEs (e. g., La, Yb and Lu, Figs. 8f-h) are strongly positively correlated with Zr in the Amdo dacites, which indicates that these elements were also essentially

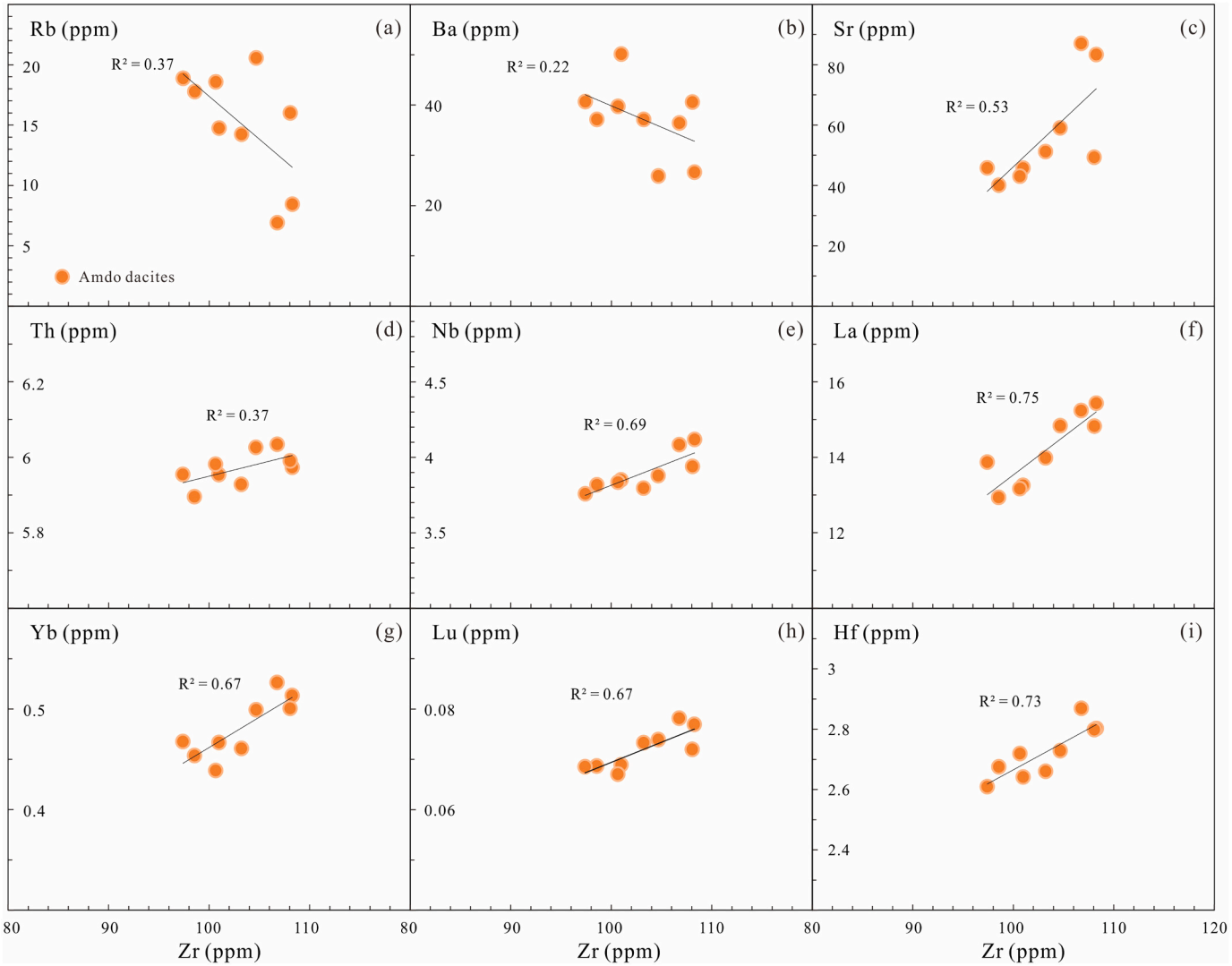


**Fig. 8.** Zr versus selected trace elements for checking element mobility during post-magmatic alteration.

immobile during post-magmatic processes. The overall similarity of the trace element patterns (Fig. 5) and homogeneous Sr-Nd-Hf isotope compositions (Fig. 6) among all the Amdo dacite samples indicates the effect of the post-magmatic modification was negligible on a whole-rock scale. We conclude that post-magmatic processes had only minor effects on the chemical compositions of the studied samples, except for a few highly mobile elements (i. e., Na, K, Rb and Ba).

#### 4.2.2. Shallow crustal contamination

Volcanic rocks that erupted in continental regions may experience shallow crustal contamination, as they ascend through the upper continental crust. The negative Nb and Ta anomalies (Fig. 5) and low contents of MgO and other compatible elements (e. g., Cr and Ni, Table S3) of the Amdo dacites probably resulted from shallow crustal assimilation. However, the Amdo dacites have much lower Nb (3.76–4.12 ppm) and Ta (0.28–0.32 ppm) concentrations than the upper continental crust (Nb = 12 ppm, Ta = 0.9 ppm; Huang et al., 2011; Rudnick and Gao, 2014) and the Neoproterozoic-Cambrian orthogneisses and Jurassic magmatic rocks (which would represent the Amdo igneous upper crustal materials; Fig. 5), the crustal contamination would largely increase their contents, thus against this probability. In addition, the Amdo dacites have lower MgO contents and Mg# than the continental crust (Rudnick and Gao, 2014), which is hard to be explained by crustal contamination.

Zr/Nb ratios remain almost constant during the magmatic process (i. e., fractional crystallization and partial melting), but change significantly during magma mixing or crustal contamination (Weaver et al., 1996). Although the Amdo dacites have a moderate range of $SiO_2$ contents (63.45–66.82 wt%; Table S3), they show a limited range of Zr/Nb ratios between 25.8 and 27.4 (Fig. 9a). These Zr/Nb ratios of the dacites are much higher than those of the continental crust, which is estimated at 13.6–16.5 (Rudnick and Gao, 2014). Therefore, the high Zr/Nb ratios of the Amdo dacites are consistent with limited or no crustal contamination.

Crustal contamination could also be revealed by whole-rock radiogenic isotope compositions (e. g., Zhang et al., 2022). The pre-existing crustal materials would be the Neoproterozoic-Cambrian orthogneisses and Jurassic magmatic and metamorphic rocks, which show very enriched Sr—Nd isotope compositions (e. g., $\varepsilon_{Nd}(t) < -10$; Fig. 6a). Contamination by these crustal materials would produce steeply negative correlations between MgO contents and initial $^{87}Sr/^{86}Sr$ ratios, and a positive correlation between MgO contents and $\varepsilon_{Nd}(t)$ values. However, the Amdo dacites show a nearly horizontal line on the $\varepsilon_{Nd}(t)$ and MgO versus $\varepsilon_{Nd}(t)$ diagram (Fig. 9b). Combine with their homogeneous trace elemental patterns and Hf isotope compositions, the shallow crustal contamination has not played a major role in the evolution of the Amdo dacites, and their Sr–Nd–Hf isotopic characteristics are inherited from their parental magmas.

#### 4.2.3. Fractional crystallization

The Amdo dacites show variable $SiO_2$ (63.45–66.82 wt%) and CaO (6.80–8.66 wt%) contents, as well as their varied Mg# values (20.0–36.1; Table S3), suggesting a common fractional crystallization process. The low Cr and Ni contents (Table S3) and negative correlations between Mg# and CaO contents (Fig. 10a) indicate that the parental magmas of the Amdo dacites probably experienced a small quantity of clinopyroxene fractionation (Huang et al., 2021a). The decreasing $Al_2O_3$ and Sr contents with decreasing Mg# (Figs. 10b-c), combined with the positive correlations between CaO and Sr contents (Fig. 10d), implies that plagioclase is a main fractional mineral phase. The absence of distinguishable Dy/Yb trends with decreasing Mg# (Fig. 10e), as well as the flat middle REE patterns in chondrite-normalized patterns are opposed to the fractionation of amphibole. Therefore, plagioclase and clinopyroxene were likely the dominant and subordinate fractionation phases in the magmatic evolution of the Amdo dacites.

### 4.3. Petrogenesis of the Amdo dacites

#### 4.3.1. Adakitic geochemical affinity

The Amdo dacites have strikingly low Mg# (20.0–36.1) and concentrations of compatible elements (e. g., Cr, Ni), which is consistent with the lower crust-derived melts (e. g., Mg# < 40; Rapp and Watson, 1995). All the samples have consistently high ratios of $(La/Yb)_N$ (20.4–21.8), and low Yb and Y contents (0.44–0.53 ppm and 5.51–6.61 ppm, respectively) (Table S3), which are similar to the geochemical definition of adakitic rocks (Fig. 11a; Castillo, 2012; Defant and Drummond, 1990; Moyen, 2009). However, the Amdo dacites show distinctly lower Sr/Y ratios (6.86–13.5) than the typical adakites (Sr/Y > 20; Castillo, 2012; Defant and Drummond, 1990) (Fig. 11b), which suggests that they were not the primary adakite melts. Given that the Sr is a highly compatible element ($D_{Sr}^{plagioclase/melt} >> 1$, D represents partition coefficient) and Y is an incompatible one ($D_{Y}^{plagioclase/melt} << 1$) in the plagioclase (Castillo, 2012; Moyen, 2009), a small amount of plagioclase fractionation would largely decrease the Sr/Y ratios of the magmas (Fig. 11b). As discussed above, the Amdo dacites experience substantial plagioclase fractionation, it is reasonable to speculate that primary melts of the Amdo dacites have the geochemical affinity of adakites.

To better evaluate the influence of plagioclase fractional crystallization on the geochemical indexes of adakites (i. e., Sr/Y and La/Yb ratios), we performed some simple trace elemental modeling based on the classic fractional crystallization model (Figs. 11a-b; Zou, 2007). The Amdo dacite sample 19AD-09 with the highest Mg# (36.1) shows the highest Sr/Y ratio (13.5) among all the samples, which represents the

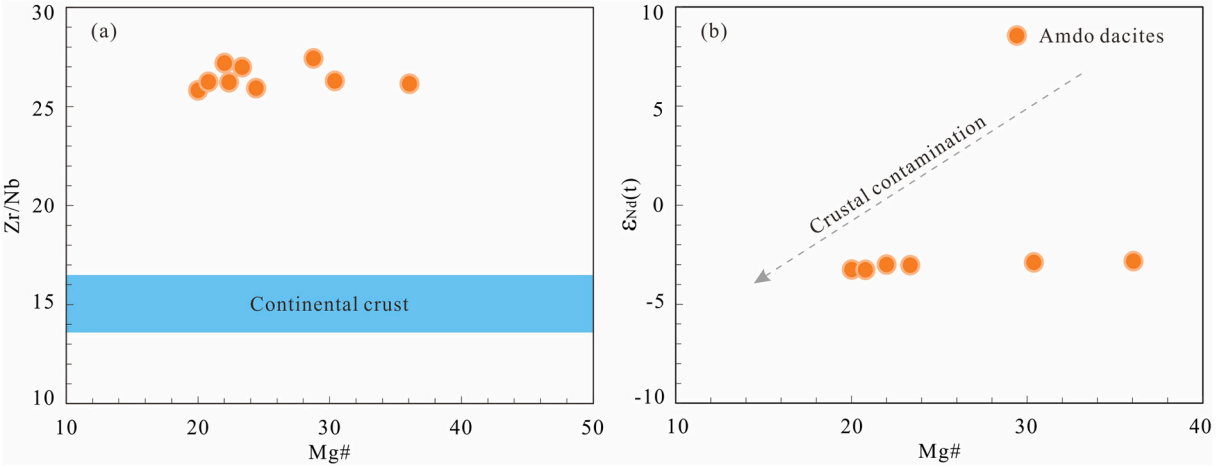


**Fig. 9.** Mg# versus (a) Zr/Nb and (b) $\varepsilon_{Nd}(t)$ diagrams showing the shallow crustal contamination for the Amdo dacites.

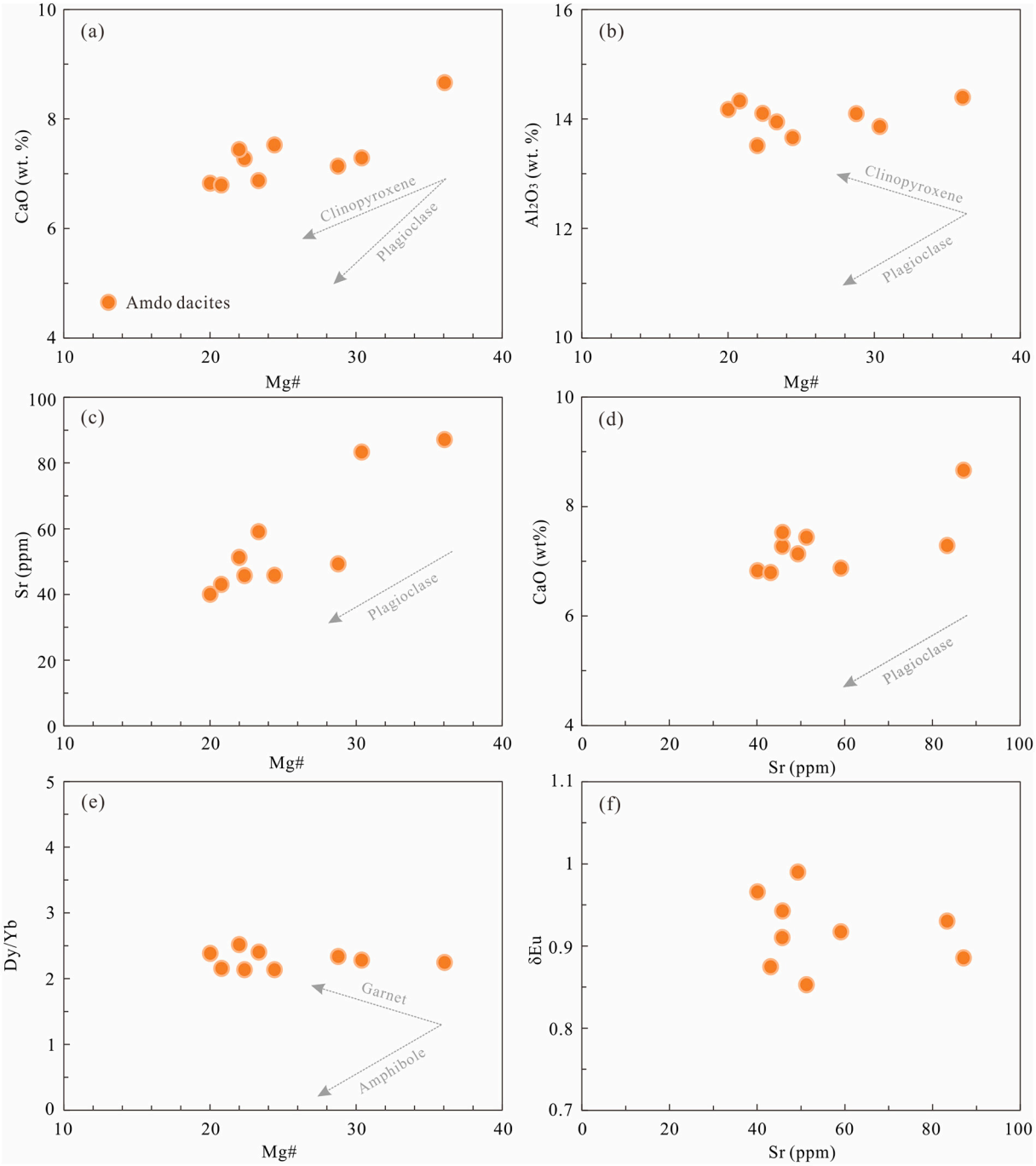


**Fig. 10.** (a) Mg# versus CaO, (b) Mg# versus $Al_2O_3$, (c) Mg# versus Sr, (d) Sr versus CaO, (e) Mg# versus Dy/Yb, (f) Sr versus δEu diagrams for the Amdo dacites.

melt composition closest to the primary adakitic magma. Therefore, we choose sample 19AD-01 as the evolutional melt during the calculation. The partition coefficients of Sr, Y, La and Yb between the plagioclase and an andesite melt were 5.28, 0.066, 0.18 and 0.1, respectively (Bacon and Druitt, 1988; Ewart and Griffin, 1994), which are used in the model because most of the primary adakitic melts are andesitic. The results indicate that nearly 10% of plagioclase added into the Amdo dacite sample would produce an adakite-like Sr/Y ratio (~20; Fig. 11b). Meanwhile, if the primary melts of the Amdo dacites are more enrichment in $SiO_2$ (e. g., dacite), the partition coefficient of Sr between the plagioclase and melt would increase to 10.7 (Ewart and Griffin, 1994), it means that <10% plagioclase fractionation would result in the low Sr/Y ratios in the Amdo dacites. The model results also exhibit that the La/Yb ratios are almost constant even though the fractionation degree of plagioclase is up to 40% (Fig. 11a), thus, the La/Yb ratios cannot be effectively changed by the fractionation of plagioclase.

It is worth noting that there is no variation in δEu with decreasing Sr concentrations in the Amdo dacites (Fig. 10f). It seems to disagree with the plagioclase fractionation, because the Eu is a highly compatible element in plagioclase (Rollinson and Pease, 2021). Previous study has attested that the partition of Eu is a strong function of oxygen fugacity, $D_{Eu}^{plagioclase/melt}$ approaches the value of $D_{Sr}^{plagioclase/melt}$ under extreme reducing conditions (Drake and Weill, 1975). In a high magmatic oxidation state, most of the Eu is present in the trivalent and is not partitioned into fractionating plagioclase, which results in a lack of a significant negative Eu anomaly (Hanson, 1980). The trace elements of

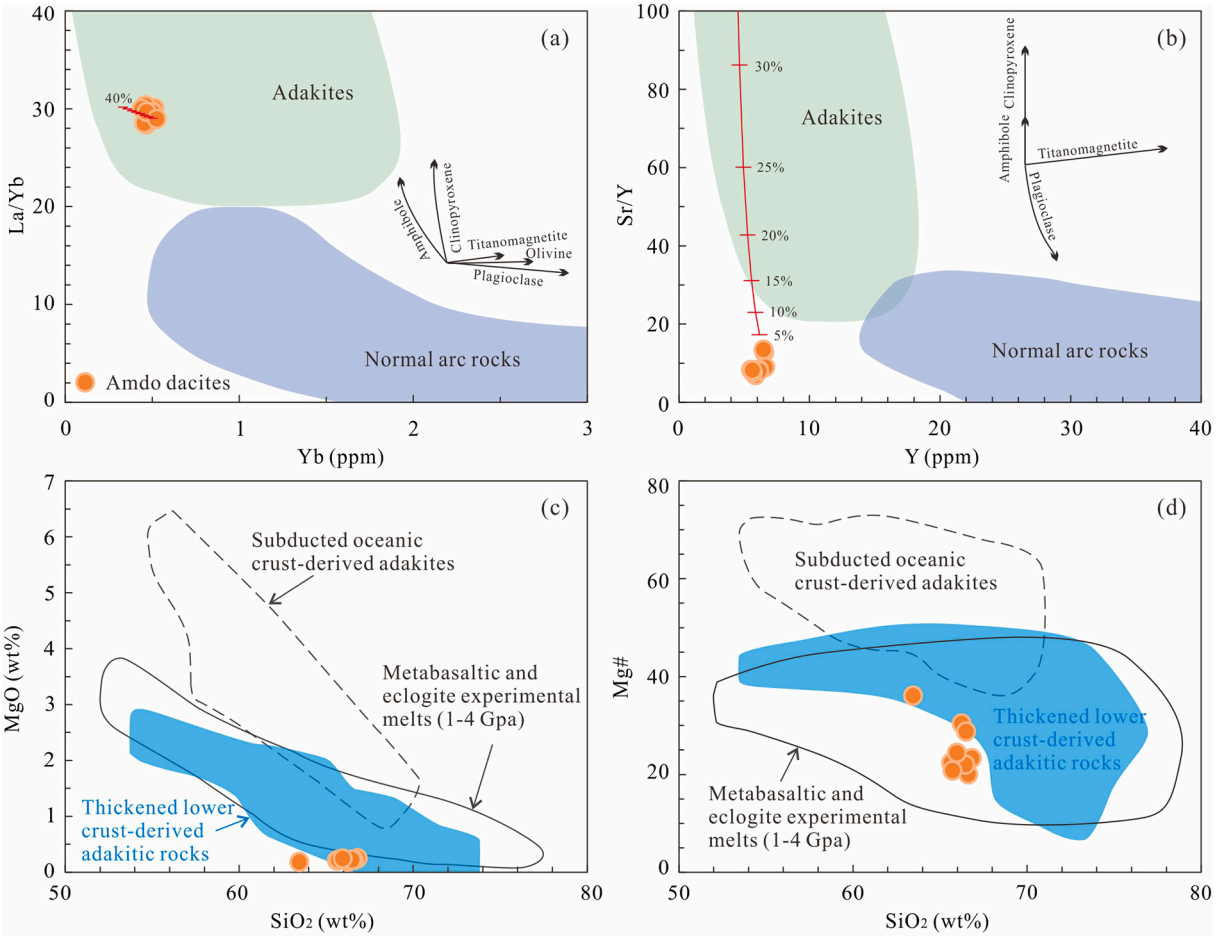


**Fig. 11.** Diagrams of (a) Yb versus La/Yb and (b) Y versus Sr/Y (Castillo, 2012) showing the adakitic rocks and the normal arc magmatic rocks. Plots of (c) $SiO_2$ versus MgO and (d) $SiO_2$ versus Mg# (modified from Wang et al., 2006) showing the sources for the adakitic rocks.

the zircons reveal that the Amdo dacites formed at a moderately oxidized environment with ΔFMQ = +0.98 (Fig. 9), which promotes $Eu^{2+}$ transform to $Eu^{3+}$ and suppresses the emergence of negative Eu anomaly (Fig. 5a). Accordingly, we propose that the Amdo dacites represent the low degree of plagioclase fractionation (<10%) production of the primary adakitic magmas with high oxygen fugacity.

*4.3.2. Genetic mechanism*

In general, the adakitic rocks could be generated from several mechanisms, including: (1) magma mixing between felsic and basaltic magmas (Guo et al., 2007); (2) the high/low-pressure fractional crystallization of parental basaltic magmas (Castillo et al., 1999; Macpherson et al., 2006); (3) melting of the subducted oceanic crust (Defant and Drummond, 1990); (4) melting of the delaminated lower continental crust (Wang et al., 2006; Xu et al., 2002); and (5) melting of the thickened lower continental crust (Wang et al., 2005).

The absence of Cretaceous mafic rocks in the Amdo microcontinent (Fig. 4), the regional deficit in rocks with similar trace element pattern, and the lack of correlation between Mg# and Nd isotope compositions in the Amdo dacites (Figs. 5 and 9b) indicate that magma mixing is not the mechanism for their formation. For the second mechanism, high-pressure fractional crystallization involving garnet will cause an increase in the Dy/Yb ratios with a decrease in the Mg# of the evolved magmas (Macpherson et al., 2006), because the heavy REEs are highly compatible in garnet. Low-pressure fractional crystallization processes usually involve amphibole and would be expected to result in positive trends for Mg# and Dy/Yb ratios (Castillo et al., 1999) as middle REEs are compatible with amphibole. However, the Dy/Yb ratios of the Amdo dacites are relatively constant with the variable Mg# (Fig. 10f). Therefore, the Amdo dacites could not have been produced by the high/low-pressure fractional crystallization of basaltic parental magma.

The partial melting of subducted oceanic crust is the original generation mechanism for adakite rocks but is not the case in this study. Although the Yb and Y contents, La/Yb ratios and fractional crystallization-corrected Sr/Y ratios of the Amdo dacites are consistent with those of classical adakites that have been generated from the subducted oceanic slab (Defant and Drummond, 1990). The Amdo dacite samples show much lower Mg# (20.0–36.1) and MgO (0.12–0.18 wt%) at given $SiO_2$ content than those adakites originated from the oceanic crust (Figs. 11c-d). In addition, the Bangong-Nujiang oceanic crust-derived adakites from Kangqiong (Li et al., 2016a) and Rena Tso (Li et al., 2016b) also show higher Mg# (32–58) and more depleted Nd isotope compositions ($\varepsilon_{Nd}(t)$ = −1.06 - 3.4) than the Amdo dacites. Moreover, the zircons of the Amdo dacites all plot into the continental zircon field rather than the oceanic crust zircon (Fig. 3d). In general, the oceanic crust-derived adakites are generated in a high temperature condition, such as the ridge subduction (e. g., Li et al., 2016a). The ridge subduction had been proposed to explain the late Jurassic (~156–148 Ma Ma) OIB-type and adakitic rocks (Li et al., 2016a, 2016b) in the western part of southern Qiangtang Terrane, whether another Early Cretaceous ridge subduction occurred in Amdo microcontinent is unknown. These lines of evidence exclude the possibility of an oceanic crust source for the Amdo adakitic dacites.

Adakitic rocks generated by the partial melting of the delaminated lower continental crust generally interact with the ambient mantle peridotite, resulting in high MgO contents (1.52–3.99 wt%) and Mg#

(40–60) (e. g., Xu et al., 2002), which is inconsistent with the Amdo dacites. Early Cretaceous was a critical stage for transformation from subduction of the Bangong-Nujiang oceanic lithosphere to Lhasa-Qiangtang continental collision (Li et al., 2020a; Zhu et al., 2016), thus it was under a compression background instead of extension for delamination. Therefore, the Amdo dacites cannot have originated from the melting of a delaminated lower continental crust.

Thickened lower crust-derived adakitic rocks are characterized by relatively low MgO contents and Mg# (Figs. 11c-d) that are similar to those of experimental melts of metabasalts and eclogites (Rapp and Watson, 1995). The low MgO contents and Mg# of the Amdo dacites are in line with the thickened lower crust-derived adakitic melts (Figs. 11c–d). Accordingly, we proposed that the thickened continental lower crust is the most likely source for the genesis of the Amdo dacites.

#### 4.3.3. Magma source

The Amdo dacites exhibit enriched and homogeneous whole-rock Sr-Nd-Hf isotope compositions ($^{87}Sr/^{86}Sr_i = 0.709796–0.710563$, $\varepsilon_{Nd}(t) = -3.27$ to $-2.82$; $\varepsilon_{Hf}(t) = 4.20–4.83$; Fig. 6), and it is plausible that they represent the melts of a thickened ancient crustal basement beneath the Amdo microcontinent (Harris et al., 1988). Most of the magmatic rocks in the Amdo microcontinent were intermediate-acidic (Fig. 4; Hu et al., 2021b; Liu, 2012; Liu et al., 2021; Wu et al., 2022; Xie, 2013; Yan et al., 2016; Yu et al., 2021; Zhang et al., 2012), consequently, the chemical compositions of the existing crustal candidates in Amdo microcontinent could be represented by the Neoproterozoic-Cambrian orthogneisses and Jurassic magmatic rocks (Figs. 1 and 6). Despite no whole-rock Sr—Nd isotope data of the Neoproterozoic orthogneisses have been reported yet, abundant zircon data of the Neoproterozoic orthogneisses show they have much lower $\varepsilon_{Hf}(t)$ than those of the Amdo dacites (Liu et al., 2021; Xie, 2013; Yu et al., 2021). The Hf isotope crustal model ages of the Neoproterozoic orthogneisses are mainly concentrated between 1.5 and 2.5 Ga, also much older than those of the Amdo dacites (0.5–1.0 Ga) (Fig. 6).

The Cambrian granitoids display more variable Sr ($^{87}Sr/^{86}Sr_i = 0.707–0.724$) and enriched Nd ($\varepsilon_{Nd}(t) = -3.4$ to $-6.3$) isotope compositions than the Amdo dacites (Harris et al., 1988; Hu et al., 2021b), suggesting that the Amdo dacites were less likely derived from the Cambrian crustal basement. In the whole-rock $\varepsilon_{Nd}(t)$ versus zircon $\varepsilon_{Hf}(t)$ diagram (Fig. 6b), the Amdo dacites also show more depleted Nd—Hf isotope compositions than the Cambrian magmatic rocks (Hu et al., 2021b; Xie, 2013). Most of the Cambrian magmatic rocks have similar zircon Hf isotope compositions compared with the Neoproterozoic orthogneisses, despite their younger Hf isotope crustal model ages (1.5–2.0 Ga) (Fig. 6c). These suggest that the latter can be a plausible source of the former with or without addition of juvenile crustal materials, whereas neither of them was the direct source for the Cretaceous Amdo dacites.

In comparison to the Cambrian granitoids, the Jurassic magmatic rocks show bimodal whole-rock Sr—Nd isotope compositions (Li et al., 2020b;Liu, 2012; Yan et al., 2016). The enriched cluster has extremely high $^{87}Sr/^{86}Sr_i$ (most between 0.720 and 0.735) and low $\varepsilon_{Nd}(t)$ ($<-10$), another cluster shows very depleted Sr—Nd isotope compositions compared to the Bangong-Nujiang oceanic ophiolites (Fig. 6c). The enriched component has lower whole-rock and zircon $\varepsilon_{Hf}(t)$ than the Amdo dacites, indicating that they would not have a similar source (Li et al., 2017; Liu et al., 2017; Zhu et al., 2011). Mixing the Sr—Nd isotope-depleted component with the enriched crustal basement has the potential to form the Amdo dacites. However, this component can derived from either the subduction Bangong-Nujiang oceanic crust (Li et al., 2020a, 2020b) or the deep asthenosphere (Liu, 2012; Yan et al., 2016). The oceanic crust-derived melts have different geochemical characteristics from the Amdo dacites (Figs. 11c-d), which have been excluded in the above discussion (see section 4.3.2). The upwelling asthenosphere could trigger massive magmatism to promote juvenile crust growth beneath the Amdo pre-existed crust. The crustal thickening and growth induced by magmatism have been widely recognized in southern Tibet (Huang et al., 2020; Mo et al., 2008; Zhu et al., 2011; Zhu et al., 2017). However, this process would result in large-scale magmatic rocks with juvenile crust-like chemical compositions (e. g., $\varepsilon_{Nd}(t) > 0$), which is at odds with the Amdo dacites. Furthermore, most of the Cretaceous magmatic rocks distributed in the Amdo microcontinent have very enriched Sr-Nd-Hf isotope compositions (Fig. 6; Liu et al., 2017; Wu et al., 2022; Zhu et al., 2011), in contrast to the model of juvenile crustal material underplating.

The Meso-Tethyan oceanic plateaus are widely distributed in the Bangong-Nujiang Ocean from the Early Jurassic to Early Cretaceous (Fig. 1), and have more depleted Sr—Nd isotopes than the Amdo ancient crustal basement (Fig. 6a; Zhang et al., 2014), which would be an alternative source component for the Amdo dacites. The mixing between the oceanic plateau materials and the Amdo crustal basement could easily explain the slightly enriched Sr—Nd isotope compositions of the Amdo dacites (Fig. 6a). A simple simulation reveals that the Sr—Nd isotopic composition of the Amdo dacites could be caused by mixing of the melts from 50 to 60% Meso-Tethyan oceanic plateaus and 50–40% Amdo ancient continental crust (Fig. 6a). In addition, the oceanic plateau materials usually have depleted Hf isotopes, which is also in accordance with the high $\varepsilon_{Hf}(t)$ of the Amdo dacites (Fig. 6d).

On the $\varepsilon_{Nd}(t)$ versus $\varepsilon_{Hf}(t)$ diagram, the Amdo dacites all plot above on the global terrestrial array ($\Delta\varepsilon_{Hf}(t) = 7.55$ to 8.43). The decoupled Nd—Hf isotopes could not be explained by the partial melting process (Fig. 6b). In general, the terrigenous sediments that plot above the Terrestrial array are deficient in zircon (with unradiogenic Hf), while coarse turbidite sands have concentrated zircon (Vervoort et al., 2011). The Amdo dacites show higher $\Delta\varepsilon_{Hf}(t)$ (7.55–8.43) than the normal arc magmatic rocks (generally <5; Fig. 6b; Vervoort et al., 2011), indicating zircon-free sediment addition. The pelagic sediments generally with zircon-deficient overlying on the oceanic plateau were likely fused to provide part of the melt for the formation of the Amdo dacites. Therefore, the Amdo dacites were derived from a hybrid source of the Amdo ancient crustal basement, the oceanic plateau, and its overlying oceanic sediments.

### 4.4. Crustal growth induced by subduction of oceanic plateau

The newly found ~117 Ma dacites in the Amdo microcontinent have arc rocks-like geochemistry characteristics (Fig. 5), as well as their similar oxidation environment ($\Delta FMQ = +0.98$; Fig. 7) and moderately magma temperature with arc magmas. There is no doubt that they were formed during the subduction of the Bangong-Nujiang oceanic plate (Fig. 12). The Amdo dacites were most likely derived from a continental lower crust made up of the ancient crustal basement and the oceanic plateau with its overlying sediments (Fig. 6a). It is reasonable to infer that the Meso-Tethyan oceanic plateaus played an important role in the crustal evolution of Amdo microcontinent. The oceanic plateau would have positive buoyancy caused by its great crustal thickness (18–40 km) and was able to be buoyantly deflected to maintain a sub-horizontal trajectory, and hence it could sequester the overlying lithosphere out of the subducted slab (Gutscher et al., 2000). This characteristic would result in the collision between the oceanic plateau and the Qiangtang Terrane and/or Amdo microcontinent, which also formed a barrier preventing magmatic activities (Zhang et al., 2021). This is consistent with the magmatic gaps formed at 148–125 Ma in the western and 160–120 Ma in the eastern segments of the BNS zone (Li et al., 2020a). This oceanic plateau-continent collision model had also been adopted by Zeng et al. (2021) and Zhang et al. (2021) to explain the magmatic lull in the Qiangtang Terrane and Beila-Nagqu area. In the case of the Amdo microcontinent, the absence of magmatism during the period of 163 to 122 Ma (Liu, 2012; Xie, 2013) could be explained by the oceanic plateau-continent collision. After the Bangong-Nujiang oceanic slab lost its buoyancy due to eclogitization of its crustal component, the slab would subduct beneath the lithosphere of the Amdo microcontinent or

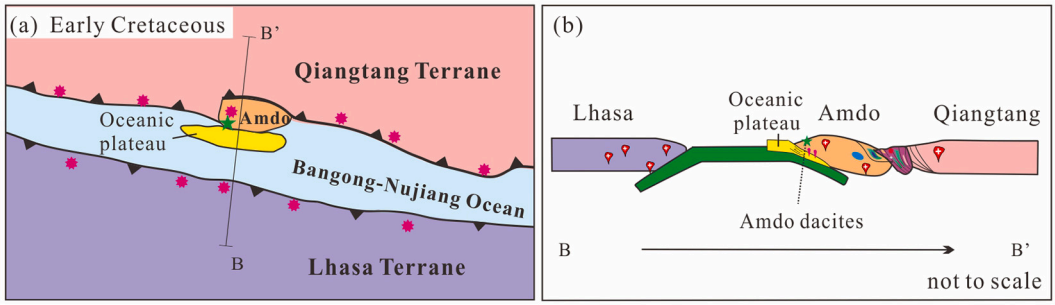


**Fig. 12.** Early Cretaceous tectonic-magmatism evolution of the Amdo microcontinent and Bangong suture zone. The Lhasa Terrane and the Amdo microcontinent experienced a double-side subduction process in the Early Cretaceous, the northward subduction of the Meos-Tethyan oceanic plateau beneath the Amdo microcontinent also occurred, which formed the Amdo dacites companying with the crustal growth (modified from Guo et al., 2022 and Peng et al., 2020).

Qiangtang Terrane and release hydrous fluids to re-ignite subduction-related magmatism. For instance, a series of Nb-rich basalts and adakites formed at 110–104 Ma in southern Qiangtang Terrane may have formed during the northward subduction of the oceanic plateau (Hao et al., 2018). Most of the Early Jurassic and Early Cretaceous oceanic plateau fragments were preserved in the south of the Amdo microcontinent, in agreement with their enormous potential for subduction (Fig. 1). Therefore, the northern subduction of the Meso-Tethyan oceanic plateau is the most likely geodynamic mechanism to explain the formation of the Amdo dacites (Fig. 12b).

While subduction and underplating of the oceanic plateaus, the overlying crust would be thickened with the transformation of mafic granulite into eclogite in the lower crust, that is, vertical growth of the continental crust (e. g., Ji et al., 2021). The wide distribution of the Meso-Tethyan oceanic plateau relicts in the Bangong-Nujiang suture zone reflects that the oceanic plateau could also directly lead to crustal thickening through obduction and accretion onto the continental margin (Zhang et al., 2014). In addition to the Early Cretaceous dacites here, Late Cretaceous (~80 Ma) adakitic volcanic rocks were found in the northern Amdo microcontinent and the southern Qiangtang Terrane (Ji et al., 2021). These Late Cretaceous volcanic rocks were explained by the relamination of the Meso-Tethyan oceanic plateaus underthrust beneath the Amdo and southern Qiangtang lithosphere (Ji et al., 2021). Although more magmatism related to oceanic plateau subduction should be further explored, the present results signify that the subduction of the oceanic plateau discontinued at least near 37 Myr. Such long-term subduction of the oceanic plateau would result in a large amount of crustal growth, which may explain the juvenile crust-like Sr-Nd-Hf isotope compositions in the intermediate-acid rocks of southern Qiangtang Terrane (e. g., Li et al., 2014; Zhu et al., 2016). Although the actual thickness of crustal growth by the oceanic plateau subduction is hard to estimate by our present study, the subduction of the oceanic plateau has certainly made a significant contribution to the crustal growth of the central Tibetan Plateau.

## 5. Conclusions

1. The Amdo dacites were generated at ca. 117 Ma and formed at a relatively low magma temperature and arc-like oxidized environment.
2. The Amdo dacites have adakitic geochemical characteristics with high La/Yb but relatively low Sr/Y ratios, which may result from the fractionation of a small volume of plagioclase.
3. The Amdo dacites were most likely derived from the thickened continental lower crust and represented a hybrid melt of the ancient crustal basement, oceanic plateau and its overlying sediments.
4. Northward subduction of the Meso-Tethyan oceanic plateau not only produced the Amdo dacites, but also played an important role in the vertical growth of the continental crust in the central Tibetan Plateau.

## Declaration of Competing Interest

The authors declare that they have no known competing financial interests or personal relationships that could have appeared to influence the work reported in this paper.

## Acknowledgments

We appreciate the Editor-in-Chief and the two anonymous reviewers for their constructive suggestions and specific comments, which greatly improved the manuscript. We thank Changqi Yang for his help in the field investigation and thank Yutong Zhang for her help during the whole-rock chemical analyses. We appreciate Hao Wang for offering the zircon standard SA01 for LA-ICP-MS U—Pb isotope dating. Feng Huang thanks the inspirational discussion with Kang Cao, Hongli Li, Xiyao Li, Pan Hu and Fanhui Pei during the preparation of the original manuscript. This research was supported by the National Natural Science Foundation of China (42121002, 41973027, 92055208 and 41730427), the Second Tibetan Plateau Scientific Expedition and Research (STEP) Program (2019QZKK0702), the National Key Research and Development Project of China (2020YFA0714800), the Fifth Bagui Scholar Innovation Project of Guangxi Province (to Jifeng Xu), Guangxi Science Innovation Base Construction Foundation (GuikeZY21195031) and the Fundamental Research Funds for the Central Universities of China (2652019054).

## Appendix A. Supplementary data

Supplementary data to this article can be found online at https://doi.org/10.1016/j.lithos.2022.106944.

## References

Bacon, C.R., Druitt, T.H., 1988. Compositional evolution of the zoned calcalkaline magma chamber of Mount-Mazama, Crater Lake, Oregon. Contrib. Mineral. Petrol. 98, 224–256.
Boehnke, P., Watson, E.B., Trail, D., Harrison, T.M., Schmitt, A.K., 2013. Zircon saturation re-revisited. Chem. Geol. 351, 324–334.
Castillo, P.R., 2012. Adakite petrogenesis. Lithos 134–135, 304–316.
Castillo, P.R., Janney, P.E., Solidum, R.U., 1999. Petrology and geochemistry of Camiguin Island, southern Philippines: insights to the source of adakites and other lavas in a complex arc setting. Contrib. Mineral. Petrol. 134, 33–51.
Condie, K.C., Kröner, A., 2013. The building blocks of continental crust: evidence for a major change in the tectonic setting of continental growth at the end of the Archean. Gondwana Res. 23, 394–402.
Corfu, F., Hanchar, J.M., Hoskin, P.W.O., Kinny, P., 2003. Atlas of zircon textures. Rev. Mineral. Geochem. 53, 469–500.
Defant, M.J., Drummond, M.S., 1990. Derivation of some modern arc magmas by melting of young subducted lithosphere. Nature 347, 662–665.
Dong, X., Zhang, Z.M., Santosh, M., Wang, W., Yu, F., Liu, F., 2011. Late Neoproterozoic thermal events in the northern Lhasa terrane, South Tibet: Zircon chronology and tectonic implications. J. Geodyn. 52, 389–405.
Drake, M.J., Weill, D.F., 1975. Partition of Sr, Ba, Ca, Y, Eu2+, Eu3+, and other REE between plagioclase feldspar and magmatic liquid: an experimental study. Geochim. Cosmochim. Ac. 39, 689–712.

Duan, M., Niu, Y.L., Sun, P., Chen, S., Kong, J.J., Li, J.Y., Zhang, Y., Hu, Y., Shao, F.L., 2022. A simple and robust method for calculating temperatures of granitoid magmas. Mineral. Petrol. 116, 93–103.
Ewart, A., Griffin, W.L., 1994. Application of proton-microprobe data to trace-element partitioning in volcanic rocks. Chem. Geol. 117, 251–284.
Fan, J.-J., Niu, Y., Liu, Y.-M., Hao, Y.-J., 2021. Timing of closure of the Meso-Tethys Ocean: Constraints from remnants of a 141−135 Ma Ocean island within the Bangong−Nujiang Suture Zone, Tibetan Plateau. GSA Bull. 133, 1875–1889.
Ferry, J.M., Watson, E.B., 2007. New thermodynamic models and revised calibrations for the Ti-in-zircon and Zr-in-rutile thermometers. Contrib. Mineral. Petrol. 154, 429–437.
Fietzke, J., Liebetrau, V., Günther, D., Gürs, K., Hametner, K., Zumholz, K., Hansteen, T. H., Eisenhauer, A., 2008. An alternative data acquisition and evaluation strategy for improved isotope ratio precision using LA-MC-ICP-MS applied to stable and radiogenic strontium isotopes in carbonates. J. Anal. At. Spectrom. 23, 955–961.
Grimes, C.B., John, B.E., Cheadle, M.J., Mazdab, F.K., Wooden, J.L., Swapp, S., Schwartz, J.J., 2009. On the occurrence, trace element geochemistry, and crystallization history of zircon from in situ ocean lithosphere. Contrib. Mineral. Petrol. 158, 757–783.
Guo, F., Nakamuru, E., Fan, W.M., Kobayoshi, K., Li, C.W., 2007. Generation of Palaeocene adakitic andesites by magma mixing; Yanji Area, NE China. J. Petrol. 48, 661–692.
Guo, R.-H., Li, S.-Z., Zhou, J., Liu, Y.-M., Yu, S.-Y., Wang, Y.-H., Liu, L., Santosh, M., 2022. The Mesozoic Amdo micro-block and East Asian superconvergent tectonic system. Gondwana Res. 101, 257–277.
Gutscher, M.A., Maury, R., Eissen, J.P., Bourdon, E., 2000. Can slab melting be caused by flat subduction? Geology 28, 535–538.
Guynn, J.H., Kapp, P., Pullen, A., Heizier, M., Gehrels, G., Ding, L., 2006. Tibetan basement rocks near Amdo reveal "missing" Mesozoic tectonism along the Bangong suture, Central Tibet. Geology 34, 505–508.
Guynn, J., Kapp, P., Gehrels, G.E., Ding, L., 2012. U–Pb geochronology of basement rocks in central Tibet and paleogeographic implications. J. Asian Earth Sci. 43, 23–50.
Hanson, G.N., 1980. Rare-earth elements in petrogenetic studies of igneous systems. Annu. Rev. Earth Pl. Sc. 8, 371–406.
Hao, L.-L., Wang, Q., Zhang, C., Ou, Q., Yang, J.-H., Dan, W., Jiang, Z.-Q., 2018. Oceanic plateau subduction during closure of the Bangong-Nujiang Tethyan Ocean: Insights from central Tibetan volcanic rocks. GSA Bull. 131, 864–880.
Harris, N.B.W., Xu, R.H., Lewis, C.L., Hawkesworth, C.J., Zhang, Y.Q., 1988. Isotope Geochemistry of the 1985 Tibet Geotraverse, Lhasa to Golmud. Philos. Trans. Royal Soc. Math. Phys. Eng. Sci. 327, 263–285.
Hu, P., Wu, Y., Bauer, A.M., Zhang, W., He, Y., 2021a. Zircon U–Pb geochronology and geochemistry of plagiogranites within a Paleozoic oceanic arc, the Erlangping unit of the Qinling accretionary orogenic belt: Petrogenesis and geological implications. Lithos 394-395, 106196.
Hu, P.-Y., Zhai, Q.-G., Zhao, G.-C., Wang, J., Tang, Y., Zhu, Z.-C., Wang, W., Wu, H., 2021b. Cambrian and Cryogenian tectonothermal events in the Amdo microcontinent, Central Tibet: Implications for paleogeographic reconstruction and tectonic evolution of northern Gondwana. Palaeogeogr. Palaeoclimatol. Palaeoecol. 569, 110332.
Hu, X., Ma, A., Xue, W., Garzanti, E., Cao, Y., Li, S.-M., Sun, G., Lai, W., 2022. Exploring a lost ocean in the Tibetan Plateau: Birth, growth, and demise of the Bangong-Nujiang Ocean. Earth Sci. Rev. 229, 104031.
Huang, H., Niu, Y., Zhao, Z., Hei, H., Zhu, D., 2011. On the enigma of Nb-Ta and Zr-Hf fractionation-a critical review. J. Earth Sci. 22, 52–66.
Huang, F., Xu, J., Wang, B., Zeng, Y., Liu, X., Liu, H., Yu, H., 2020. Destiny of Neo-Tethyan Lithosphere during India-Asia Collision. Earth Sci. 45, 2785–2804.
Huang, F., Rooney, T.O., Xu, J.-F., Zeng, Y.-C., 2021a. Magmatic record of continuous Neo-Tethyan subduction after initial India-Asia collision in the central part of southern Tibet. GSA Bull. 133, 1600–1612.
Huang, F., Zhang, Z., Xu, J., Li, X., Zeng, Y., Xu, R., Liu, X., Zhang, L., Zhang, M., Yang, C., Zhang, L., Yu, H., Yang, X., 2021b. Lithospheric extension in response to subduction of the Paleo-Pacific Plate: Insights from early Jurassic intraplate volcanic rocks in the Sk2 Borehole, Songliao Basin, NE China. Lithos 380-381, 105871.
Ji, C., Yan, L.-L., Lu, L., Jin, X., Huang, Q., Zhang, K.-J., 2021. Anduo late cretaceous high-K calc-alkaline and shoshonitic volcanic rocks in Central Tibet, western China: Relamination of the subducted Meso-Tethyan oceanic plateau. Lithos 400-401, 106345.
Li, J.-X., Qin, K.-Z., Li, G.-M., Richards, J.P., Zhao, J.-X., Cao, M.-J., 2014. Geochronology, geochemistry, and zircon Hf isotopic compositions of Mesozoic intermediate–felsic intrusions in Central Tibet: Petrogenetic and tectonic implications. Lithos 198–199, 77–91.
Li, Y., He, J., Han, Z., Wang, C., Ma, P., Zhou, A., Liu, S.-A., Xu, M., 2016a. Late Jurassic sodium-rich adakitic intrusive rocks in the southern Qiangtang terrane, central Tibet, and their implications for the Bangong–Nujiang Ocean subduction. Lithos 245, 34–46.
Li, S.-M., Zhu, D.-C., Wang, Q., Zhao, Z., Zhang, L.-L., Liu, S.-A., Chang, Q.-S., Lu, Y.-H., Dai, J.-G., Zheng, Y.-C., 2016b. Slab-derived adakites and subslab asthenosphere-derived OIB-type rocks at 156 ± 2 Ma from the north of Gerze, central Tibet: Records of the Bangong–Nujiang oceanic ridge subduction during the Late Jurassic. Lithos 262, 456–469.
Li, H.-Q., Xu, Z.-Q., Webb, A.A.G., Li, T.-F., Ma, S.-W., Huang, X.-M., 2017. Early Jurassic tectonism occurred within the Basu metamorphic complex, eastern Central Tibet: Implications for an archipelago-accretion orogenic model. Tectonophysics 702, 29–41.
Li, S.-M., Wang, Q., Zhu, D.-C., Cawood, P.A., Stern, R.J., Weinberg, R., Zhao, Z., Mo, X.-X., 2020a. Reconciling orogenic drivers for the evolution of the bangong-nujiang tethys during middle-late jurassic. Tectonics 39, e2019TC005951.
Li, M.-J., Zeng, Y.-C., Xu, J.-F., Huang, F., Chen, Q., 2020b. Petrogenesis of Early Jurassic (ca. 181 Ma) dacitic–rhyolitic volcanic rocks in the Amdo ophiolite mélange, central Tibetan Plateau: Low-pressure partial melts of Bangong–Nujiang Tethys oceanic crust? Geol. J. 55, 3283–3296.
Liu, M., 2012. Petrogenesis and Tectonic Significance of Early Jurassic Alkalic Pluton in Nyainrong Microcontinent, Central Tibet. School of Earth Science and Resources. China University of Geosciences Beijing, Beijing, China, pp. 1–169.
Liu, D., Shi, R., Ding, L., Huang, Q., Zhang, X., Yue, Y., Zhang, L., 2017. Zircon U–Pb age and Hf isotopic compositions of Mesozoic granitoids in southern Qiangtang, Tibet: Implications for the subduction of the Bangong–Nujiang Tethyan Ocean. Gondwana Res. 41, 157–172.
Liu, Y., Wang, Y., Li, S., Santosh, M., Guo, R., Yu, S., 2021. Neoproterozoic Amdo and Jiayuqiao microblocks in the Tibetan Plateau: Implications for Rodinia reconstruction. GSA Bull. 133, 663–678.
Liu, Y., Li, S., Zhai, Q., Tang, Y., Hu, P., Guo, R., Liu, Y., Wang, Y., Yu, S., Cao, H., Zhou, J., Wang, G., 2022. Jurassic tectonic evolution of Tibetan Plateau: a review of Bangong-Nujiang Meso-Tethys Ocean. Earth Sci. Rev. 227, 103973.
Loucks, R.R., Fiorentini, M.L., Henriquez, G.J., 2020. New magmatic oxybarometer using trace elements in zircon. J. Petrol. 61, egaa034.
Lu, L., Wu, Z., Zhao, Z., Hu, D., Ye, P., 2014. Zircon SHRIMP U-Pb dating, geochemical characteristics and tectonic significance of granitic gneisses in Amdo, Tibet. J. Earth Sci. 25, 473–485.
Lu, L., Yan, L., Li, Q., Zeng, L., Jin, X., Zhang, Y., Hou, Q., Zhang, K., 2016. Oceanic plateau and its significances on the Earth system: a review. Acta Petrol. Sin. 32, 1851–1876.
Macpherson, C.G., Dreher, S.T., Thirlwall, M.F., 2006. Adakites without slab melting: High pressure differentiation of island arc magma, Mindanao, the Philippines. Earth Planet. Sci. Lett. 243, 581–593.
Mo, X.X., Niu, Y.L., Dong, G.C., Zhao, Z.D., Hou, Z.Q., Zhou, S., Ke, S., 2008. Contribution of syncollisional felsic magmatism to continental crust growth: a case study of the Paleogene Linzizong volcanic Succession in southern Tibet. Chem. Geol. 250, 49–67.
Moyen, J.F., 2009. High Sr/Y and La/Yb ratios: the meaning of the "adakitic signature". Lithos 112, 556–574.
Peng, Y., Yu, S., Li, S., Liu, Y., Santosh, M., Lv, P., Li, Y., Xie, W., Liu, Y., 2020. The odyssey of Tibetan Plateau accretion prior to Cenozoic India-Asia collision: probing the Mesozoic tectonic evolution of the Bangong-Nujiang Suture. Earth Sci. Rev. 211, 103376.
Peng, Y., Yu, S., Li, S., Liu, Y., Santosh, M., Lv, P., Li, Y., Li, C., Liu, Y., 2022. Tectonic erosion and deep subduction in Central Tibet: evidence from the discovery of retrograde eclogites in the Amdo microcontinent. J. Metamorph. Geol. https://doi.org/10.1111/jmg.12685.
Rapp, R.P., Watson, E.B., 1995. Dehydration melting of metabasalt at 8-32-Kbar - implications for continental growth and crust-mantle recycling. J. Petrol. 36, 891–931.
Richards, J.P., 2022. Porphyry copper deposit formation in arcs: what are the odds? Geosphere 18, 130–155.
Rollinson, H., Pease, V., 2021. Using Geochemical Date to Understand Geological Processes. Cambridge University Press, Cambridge, UK, pp. 1–290.
Rudnick, R.L., Gao, S., 2014. Composition of the continental crust. In: Rudnick, R.L. (Ed.), Treatise on Geochemistry. Elsevier, pp. 1–51.
Stern, C.R., 2020. The role of subduction erosion in the generation of Andean and other convergent plate boundary arc magmas, the continental crust and mantle. Gondwana Res. 88, 220–249.
Sun, S., McDonough, W.F., 1989. Chemical and isotopic systematics of oceanic basalts: implications for mantle composition and processes. Geol. Soc. Lond., Spec. Publ. 42, 313–345.
Vervoort, J.D., Plank, T., Prytulak, J., 2011. The Hf–Nd isotopic composition of marine sediments. Geochim. Cosmochim. Acta 75, 5903–5926.
Vogt, K., Gerya, T.V., 2014. From oceanic plateaus to allochthonous terranes: Numerical modelling. Gondwana Res. 25, 494–508.
Wang, Q., McDermott, F., Xu, J.F., Bellon, H., Zhu, Y.T., 2005. Cenozoic K-rich adakitic volcanic rocks in the Hohxil area, northern Tibet: Lower-crustal melting in an intracontinental setting. Geology 33, 465–468.
Wang, Q., Wyman, D.A., Xu, J.F., Zhao, Z.H., Jian, P., Xiong, X.L., Bao, Z.W., Li, C.F., Bai, Z.H., 2006. petrogenesis of cretaceous adakitic and shoshonitic igneous rocks in the luzong area, anhui province (eastern china): implications for geodynamics and cu-au mineralization. lithos 89, 424–446.
Wang, B.-D., Wang, L.-Q., Chung, S.-L., Chen, J.-L., Yin, F.-G., Liu, H., Li, X.-B., Chen, L.-K., 2016. Evolution of the Bangong–Nujiang Tethyan ocean: Insights from the geochronology and geochemistry of mafic rocks within ophiolites. Lithos 245, 18–33.
wang, x.-c., li, q., wilde, s.a., li, z.-x., li, c., lei, k., li, s.-j., li, l., pandit, m.k., 2021a. Decoupling between oxygen and radiogenic isotopes: evidence for generation of juvenile continental crust by partial melting of subducted oceanic crust. J. Earth Sci. 32, 1212–1225.
Wang, B., Wang, L., Zhou, D., Wang, D., Yu, Y., Yan, G., Wu, Z., 2021b. Longmu Co-Shuanghu-Changning-Menglian suture zone: the boundary between Gondwanaland and Pan-Cathaysia mainland in the Qinghai-Tibet Plateau. Geol. Bull. China 40, 1783–1798.
Watson, E.B., Harrison, T.M., 1983. Zircon saturation revisited: temperature and composition effects in a variety of crustal magma types. Earth Planet. Sci. Lett. 64, 295–304.

Weaver, B., Kar, A., Davidson, J., Colucci, M., 1996. Geochemical characteristics of volcanic rocks from Ascension island, South Atlantic Ocean. Geothermics 25, 449–470.
Wu, K., Zhong, Y., Yuan, Y., Wan, Z., Xia, B., Wu, T., 2022. Early cretaceous Granitoids Magmatism in the Nagqu Area, Northern Tibet: Constraints on the timing of the Lhasa-Qiangtang Collision. Minerals 12, 933.
Xie, C., 2013. Tectonic Evolution of the Nyainrong Microcontinent. Tibet-constrains from geochronology and geochemistry. Jilin University, Changchun, China, pp. 1–151.
Xu, J.F., Shinjo, R., Defant, M.J., Wang, Q., Rapp, R.P., 2002. Origin of Mesozoic adakitic intrusive rocks in the Ningzhen area of East China: Partial melting of delaminated lower continental crust? Geology 30, 1111–1114.
Yan, H., Long, X., Wang, X.-C., Li, J., Wang, Q., Yuan, C., Sun, M., 2016. Middle Jurassic MORB-type gabbro, high-Mg diorite, calc-alkaline diorite and granodiorite in the Ando area, Central Tibet: evidence for a slab roll-back of the Bangong-Nujiang Ocean. Lithos 264, 315–328.
Yu, Y.P., Xie, C.M., Dong, Y.S., Dong, Y.C., Wang, B., Duan, M.L., Song, Y.H., 2021. Early Neoproterozoic granitic gneisses in the Amdo micro-continent, Tibet: petrogenesis and geodynamic implications. Int. Geol. Rev. 63, 342–356.
Zeng, Y.C., Xu, J.F., Chen, J.L., Wang, B.D., Huang, F., Xia, X.P., Li, M.J., 2021. Early cretaceous (~138–134 Ma) forearc ophiolite and tectonomagmatic patterns in central tibet: subduction termination and re-initiation of meso-tethys ocean caused by collision of an oceanic plateau at the continental margin? Tectonics 40, e2020TC006423.
Zhang, Z.M., Dong, X., Liu, F., Lin, Y.H., Yan, R., Santosh, M., 2012. Tectonic evolution of the amdo terrane, central tibet: Petrochemistry and Zircon U-Pb geochronology. J. Geol. 120, 431–451.
Zhang, K.J., Xia, B., Zhang, Y.X., Liu, W.L., Zeng, L., Li, J.F., Xu, L.F., 2014. Central Tibetan Meso-Tethyan oceanic plateau. Lithos 210, 278–288.
Zhang, W.Q., Liu, C.Z., Liu, T., Zhang, C., Zhang, Z.Y., 2021. Subduction initiation triggered by accretion of a Jurassic oceanic plateau along the Bangong–Nujiang Suture in central Tibet. Terra Nova 33, 150–158.
Zhang, Y., Huang, F., Xu, J., Zeng, Y., Wang, B., Lv, M., Zhang, L., Li, M., Zhang, Z., Tian, Y., Liu, Q., Zhang, L., 2022. Origin of the volcanic rocks in Dianzhong Formation, Central Lhasa Terrane, Tibet: implication for the genesis of syn-collisional magmatism and Neo-Tethyan slab roll-back. Int. Geol. Rev. https://doi.org/10.1080/00206814.2022.2031314.
Zhu, D.C., Zhao, Z.D., Niu, Y.L., Mo, X.X., Chung, S.L., Hou, Z.Q., Wang, L.Q., Wu, F.Y., 2011. The Lhasa Terrane: Record of a microcontinent and its histories of drift and growth. Earth Planet. Sci. Lett. 301, 241–255.
Zhu, D.-C., Zhao, Z.-D., Niu, Y., Dilek, Y., Hou, Z.-Q., Mo, X.-X., 2013. The origin and pre-Cenozoic evolution of the Tibetan Plateau. Gondwana Res. 23, 1429–1454.
Zhu, D.-C., Li, S.-M., Cawood, P.A., Wang, Q., Zhao, Z.-D., Liu, S.-A., Wang, L.-Q., 2016. Assembly of the Lhasa and Qiangtang terranes in Central Tibet by divergent double subduction. Lithos 245, 7–17.
Zhu, D.C., Wang, Q., Cawood, P.A., Zhao, Z.D., Mo, X.X., 2017. Raising the Gangdese Mountains in southern Tibet. J. Geophys. Res.-Sol. Ea. 122, 214–223.
Zou, H., 2007. Quantitative Geochemistry. Imperial College Press, London, pp. 1–287.